Chapter 7

# On the Prospects of Using Metallic Glasses for In-vessel Mirrors for Plasma Diagnostics in ITER

Vladimir S. Voitsenya, Alexandra F. Bardamid, Martin Balden, Flaviu Gostin, Sergey V. Khovrich, Vladimir G. Konovalov, Konstantin V. Kovtun, Petro M. Lytvyn, Sergey V. Ketov, Dmitri V. Luzguine-Luzgin, Sergei I. Solodovchenko, Anatoly N. Shapoval, Anatoly F. Shtan', Vladislav N. Bondarenko, Ivan V. Ruzhkov, Ol'ga O. Skoryk and Andrei A. Vasil'ev

Additional information is available at the end of the chapter

http://dx.doi.org/10.5772/63885

**Abstract**

This chapter reviews main results obtained on mirror-like samples made of several grades of bulk metallic glasses (BMG). Experiments were carried out under simulated conditions typical for the operation of plasma facing in-vessel mirrors of optical plasma diagnostics in fusion reactor ITER. Bombardment with $D^0$ and $T^0$ atoms radiated from burning plasma was predicted to be the main reason for the degradation of optical properties of such mirrors. Therefore, to simulate the behavior of mirrors in ITER, mirror-like samples were subjected to bombardment by ions of deuterium plasma with fixed or wide energy distribution. The effects of ion bombardment on optical properties, development of roughness, uptake of deuterium, appearance of blisters, and manifestation of some chemical processes are presented and discussed.

**Keywords:** amorphous mirrors, sputtering effects, deuterium uptake, chemical processes, blister-like features

## 1. Introduction

In the experimental fusion reactor ITER, many different methods of plasma diagnostics are envisaged to be used [1]. A big portion of methods are intended for optical measurements, and these have to be based on reflective optics, because of the high level of deeply penetrating radiations, gammas, and neutrons, which may degenerate the refractive optics components. The mirrors facing the burning plasma (first mirrors, FM) will be additionally subjected to fluxes of charge-exchange atoms (CXA, mainly $D^0$ and $T^0$ atoms) with a wide energy distribution, up to several hundred eV [2]. To overcome negative effects of CXA sputtering on mirror characteristics (due development of surface roughness), it was decided to fabricate first mirrors for ITER from single crystal (SC) metal, and molybdenum is the first candidate as a FM material.

At present, it is not known which effect the simultaneous irradiation of the FM surface with neutrons and CXA will have. However, there is a probability that a single crystal will lose its ideal SC structure what would result in gradual development of roughness (under CXA bombardment) and degradation of optical properties.

A real alternative to SC mirrors can be mirrors fabricated from amorphous metal alloys (bulk metallic glasses, BMGs). They do not have any arranged structure larger than a few nanometer and therefore may be more resistive under irradiation with neutrons in comparison with crystallized metals. Recent results on simulating the neutron irradiation effects by exposing BMG samples with 3 MeV $Ni^+$ ions did not lead to big degradation of hardness and Young's modulus in the dose range of 0.1–10 dpa [3,4]. It is important to note that the structure of samples has continued to be amorphous, without indication of appearance of crystallization.

Additionally, due to the lack of crystallized structure, under long-term sputtering, a polished BMG mirror has to resemble a liquid under evaporation: its surface has to be smooth regardless of sputtering time. Such assumption was mentioned in [5] and has found support later, after appearance of technology to produce BMG casts with size (≥10 mm) sufficient for the fabrication of mirror samples to provide corresponding experiments. Zr-based BMGs reveal relatively high crystallization temperature compared with other BMGs. From a practical standpoint, the glass forming ability of Zr-based BMGs is very good enabling the manufacturing of fully glassy components with thickness values in excess of 10 mm.

This chapter is a short review of main results obtained with BMG mirror samples in experiments that partly simulate the conditions for FM operation in ITER, that is, long-term sputtering by ions of deuterium plasma (in some cases by ions of argon plasma) with energy from 60 eV up to 1350 eV. Mirror samples were fabricated from five BMG grades (**Table 1**). The program of experiments with each BMG grade was not identical, and thus, new information was obtained, and some new properties of BMGs were found for both amorphous and crystallized BMG specimens. This chapter presents results on the following: (1) effects of long-term ion sputtering on optical properties of mirror-like BMG samples, (3) effects of deuterium adsorption, (4) the role of chemical processes on BMG surface when the deuterium plasma is contaminated with oxygen, and (5) observation of blister-like features due to deuterium exposure.

http://dx.doi.org/10.5772/63885

In Section 2, the specimens and the experimental details regarding the plasma exposures and characterization are described. Section 3 contains the main results on changes due to plasma exposure, in particular deuterium adsorption, reflectance, and erosion rate and the differences due to the state, amorphous or crystallized by annealing. In Section 4, some concluding remarks are provided. Appendix A contains details on BMG sample preparation in NSC KIPT (Kharkov, Ukraine), and in Appendix B, the results of processing of an image of laser beam after reflection from amorphous and crystallized mirrors are shown.

## 2. Experimental and precharacterization

### 2.1. Descriptions of specimens

A list of all grades of samples with their composition, shape, and size is presented in **Table 1**.

| Grade # | Composition | Size, mm |
|---|---|---|
| 1 (Vit1-LM) | Zr41.2Ti13.8Cu12.5Ni10Be22.5 | Ø22 × 3 |
| 2 (Vit1-NSC) | Zr41.2Ti13.8Cu12.5Ni10Be22.5 | Ø22 × 3 |
| 3 (Vit4) | Zr46.75Ti8.25Cu7.5Ni10Be27.5 | Ø5 × 3 |
| 4 | Zr48Cu36Al8Ag8 | Ø(16–22) × 2 |
| 5 (Vit106) | Zr57Cu15.4Al10Ni12.6Nb5 | 20 × 22 |

**Table 1.** List of grades with composition given in at.%.

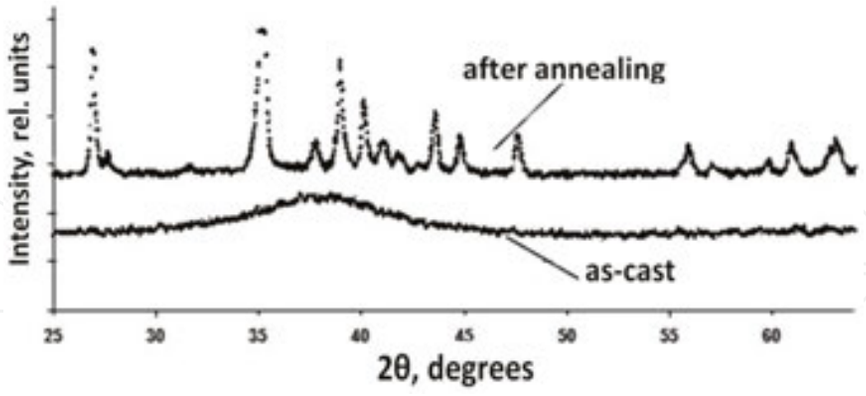


**Figure 1.** Results of X-ray diffraction measurements obtained with the half of the amorphous sample of grade #2 (lower curve) and the half annealed at 773°K during 1 hour.

Three BMG samples of **grade #1** produced by Liquidmetal Co (USA) and three billets of **grade #2** have the same nominal composition.

The billets of grade #2 were casted as discs with diameter ~26 and ~8 mm in thickness (the details of their fabrication in NSC KIPT are described in Appendix A). They were cut into

approximately equal halves (final size Ø22 × 3 mm): one half of every billet was left amorphous and the second half was annealed (1 hour at 773°K) to have a fine-crystalline material. Thus, for this grade, there was a possibility to compare the behavior of mirrors from the identical material but with different structures, amorphous and fine-crystalline. The X-ray data on the structure of such a pair are shown in **Figure 1**.

The position of the peaks in a diffractogram indicated the existence of the following nano-crystals: $Zr_2Ni$, $Ti_2Ni$, $Zr_2Cu$, and $Zr_xCu_y$ with $x$ and $y$ exceeding two. By measuring the half-width of the peaks, the size of crystallites was roughly estimated to 50 nm using the following formula [6]:

$$D = \frac{0.9\,\lambda}{\beta \cos\theta} \tag{1}$$

where $\lambda$ is the X-ray wavelength, $\theta$ is the Bragg angle, and $\beta$ is the full width at half maximum of the diffraction peak.

After crystallization of three halves, all three pairs of grade #2 were polished simultaneously.

The mirror specimens of **grade #3** (more than 10 pieces) were cut from a 5-mm-diameter rod to discs of 3 mm thickness. Because of the small surface area, they were not used for some experiments, namely for measuring the absorptivity of deuterium.

The cast of **grade #4** had a complicated shape; therefore, the mirror samples (five pieces) had different diameter from Ø16 to Ø22 mm with thickness of 2 mm each.

The cast of **grade #5** was of rectangular shape; after cutting it into two samples the size of mirror specimens became 20 × 22 × 3 mm.

XRD (X-ray diffraction) analysis confirmed the glassy state of all samples (diffraction patterns not shown here).

All prepared billets were polished to a high optical quality.

### 2.2. Pretreatment and initial reflectance

Prior to exposure experiments, all mirror samples were initially cleaned for ≥20 min with low-energy deuterium plasma ions, $E_i$ ~ 60 eV or sometimes with low-energy Ar plasma ions, to remove the organic film appeared due to rinsing of samples in acetone and alcohol after the polishing. The reflectance of mirror samples after this exposure was taken as their initial spectral reflectance.

The comparison of initial reflectance, $R_0(\lambda)$, for one BMG mirror specimens of each grade is presented in **Figure 2** together with W and Mo reflectivity data from [7]. The measurements were done in the wavelength range 220–650 nm at normal incidence of the light by the use of a two-channel method described in [8] with a homemade attachment to a standard mono-chromator.

http://dx.doi.org/10.5772/63885

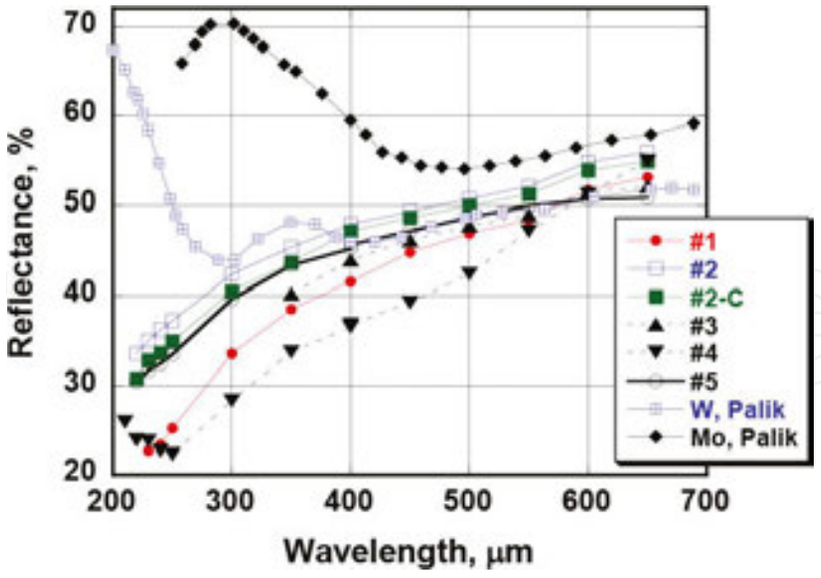


**Figure 2.** Initial reflectance $R_0(\lambda)$ measured just after cleaning by low-energy ions of deuterium or argon plasma of samples of the five grades together with the data for W and Mo from literature [7].

The $R_0(\lambda)$ values of some BMG mirror samples are close to $R_0(\lambda)$ values of tungsten for the wavelengths range ~400–700 nm and is approaching to the reflectance of Mo mirror at $\lambda > 600$ nm. Crystallization does not lead to any significant change of initial optical properties of samples in the wavelength interval of measurements (220–650 nm), as can be concluded from comparing the data for grades #2 and #2-C (crystallized).

### 2.3. Heterogeneities observed in the body of BMG samples

After the last polishing procedure, some local peculiarities were discovered on smooth sample surfaces of the grade #1. Such peculiarities were not observed on the other grades.

Their level was a little below the main surface, appear usually as a group, are roughly of oval shape, distributed over the main surface of mirror sample more or less uniformly, and are observable in both, optical microscope and scanning electron microscope (SEM). The total relative area of these inhomogeneities was estimated to be at the level of ~1%, so they did not have any essential influence on measurement of reflectance, that is, the performance of the mirror. The fact of their elevation below the matrix supposed that the composition of these features differs from that of the main volume of material and that their hardness again mechanical treatment is inferior to the hardness of the bulk.

**Figure 3** shows two SEM images of the same region obtained by different detectors of SEM, detecting (a) mainly secondary electrons and (b) backscattered electrons. In the first case, the contrast of the image is mainly determined by the surface topography, but in the second regime, the contrast occurs due to differences in the atomic number of the surface elements. In this second case, the domains with predominance of light elements appear darker than the surrounding; therefore, we may state that the recessed domains are enriched by the lighter component of the material (the average atomic number here is below that of the matrix).

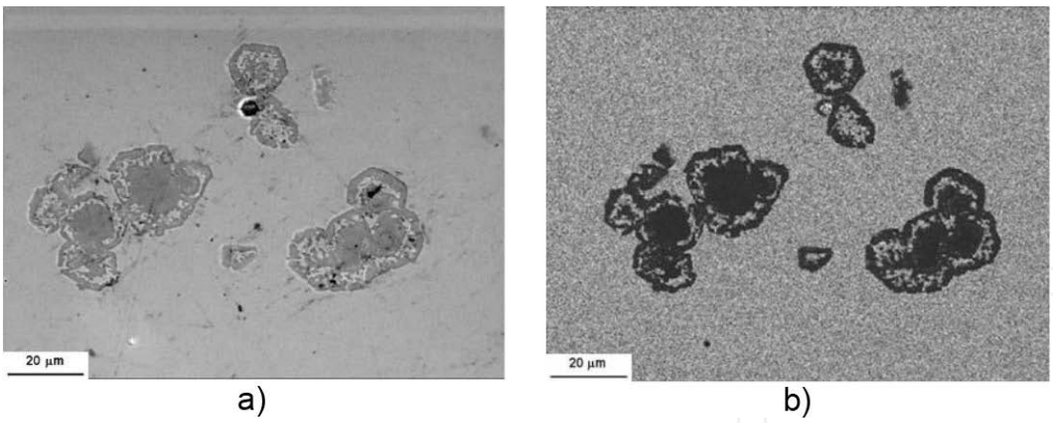


**Figure 3.** SEM images from secondary (a) and backscattered electrons (b) of inhomogeneities on the sample surface of grade #1 [9].

Under ion bombardment, as a result of the sputtering process, initially lower parts of the surface descended deeper below the main level and turned into shallow holes with a rather nonplanar bottom shown in **Figure 4**. The depth of holes increased with increase in ion fluence, which indicates (i) a lower resistance of these inclusions to ion sputtering and (ii) their volumetric character.

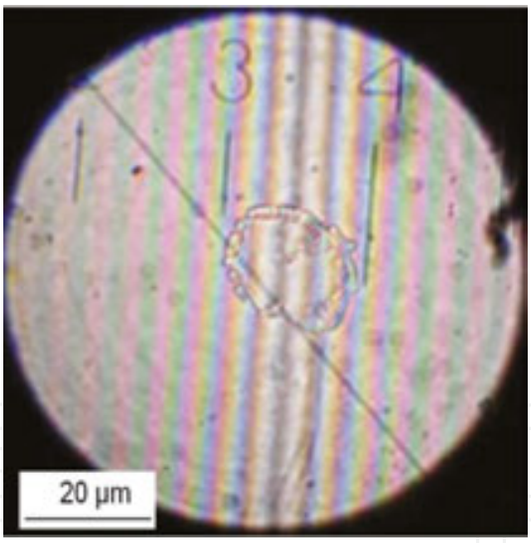


**Figure 4.** Photograph of interferometer microscope after the layer of ~2 μm was sputtered with deuterium plasma ions [10]. The interference fringes indicate a depth of ~150 nm fort the central feature.

The difference in composition of the material inside the inhomogeneities and the surrounding matrix was confirmed by the following two methods: an electron microprobe analysis (**Table 2**) and scanning electron microscope (SEM) with energy-dispersive X-ray spectroscopy (EDX), **Figure 5**. The data of microprobe analysis demonstrate that the material in the holes is depleted in zirconium (Zr) and titanium (Ti), and enriched with the other elements such as copper and nickel. From this result, it is not surprising that the rate of sputtering of the inhomogeneities

http://dx.doi.org/10.5772/63885

is higher than of the matrix. Taking into account, the sputtering yields, $Y$, of components of the mirror material [11] one can find for deuterium ions at energy 1000 eV, $Y(Zr)=5.5\times10^{-3}$ at/ion, is about one order of magnitude lower than $Y$(Be), $Y$(Cu), $Y$(Ni), and two times lower than $Y$(Ti). At lower ion energy, the difference in sputtering yields is much greater. The microprobe data show that after long-term sputtering the composition of Zr in holes continues to be below that in the matrix.

| Element | Nominal composition (at.%) | Matrix composition (at.%) | Inhomogeneity composition (at.%) |
|---|---|---|---|
| Zr | 41.2 (100%) | 52.8 (100%) | 43.0 (100%) |
| Ti | 13.8 (33.2%) | 17.4 (33%) | 12.0 (28%) |
| Cu | 12.5 (30%) | 15.2 (28.8%) | 24.3 (56.5%) |
| Ni | 10 (24%) | 14.6 (27.7%) | 20.7 (43%) |
| Be | 22.5 (54.9%) | | |

**Table 2.** Elemental composition of the mirror material from grade #1: nominal (second column) and measured by means of microprobe method in the matrix and in the inhomogeneity (without taking into account Be). Ratio to the Zr content is given in brackets [10].

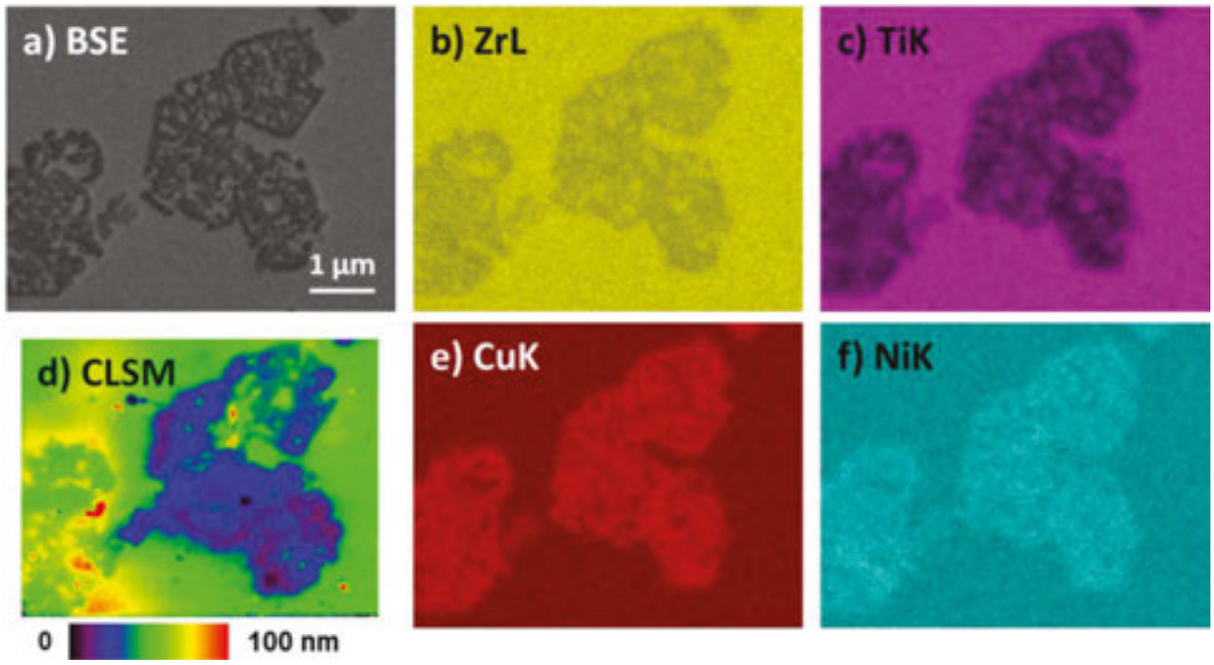


**Figure 5.** (a) SEM image from backscattered electrons and (b, c, e, f) the corresponding elemental maps obtained by EDX of the polished mirror surface of a sample of grade #1. (d) Height plot obtained by confocal laser scanning microscopy.

Comparing the EDX maps for zirconium, nickel, copper, and titanium (**Figure 5**), one could see that for inhomogeneities of the hole type, the intensities of ZrL and TiK lines are in anticorrelation with intensities of CuL and NiL lines what is in agreement with the results of

microprobe analysis. The data obtained by confocal laser scanning microscopy, **Figure 5d**, indicate that inhomogeneity is below the matrix level.

As **Figure 6** shows, the alloys grades #3 and #4 also contain heterogeneities, however of another kind. The majority of the heterogeneities have a dendritic appearance. On one occasion, a rather full structure of such an inhomogeneity was revealed after bombardment of one of grade #3 samples with argon ions, **Figure 6a**. Its shape is quite similar to the shape of crystals described by the authors of this alloy [12] (see also references ibidem). Important, the surface between these features is continuing to be smooth.

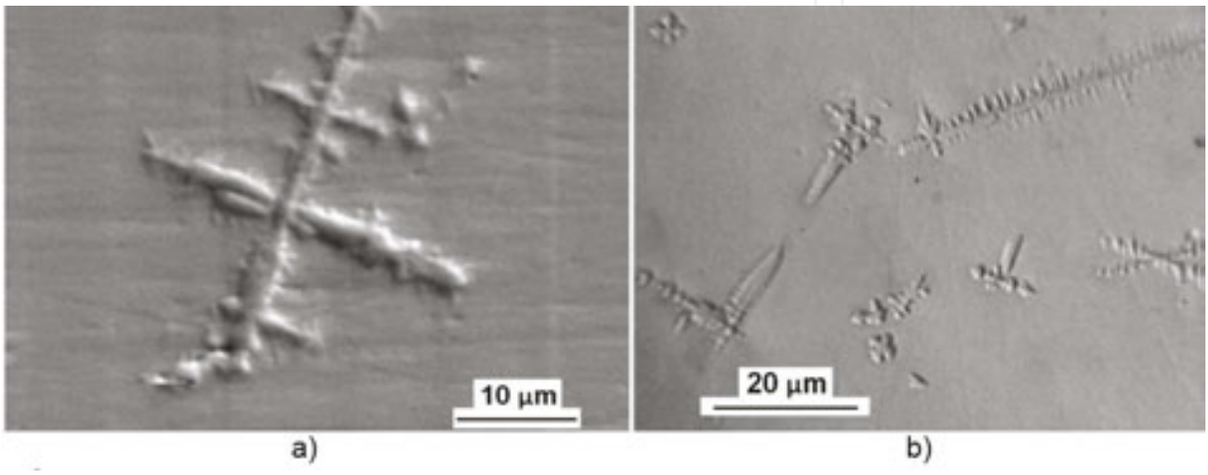


**Figure 6.** SEM images of the mirror surface: (a) sample of grade #3 after sputtering with argon ions of the layer of ~5 μm, (b) sample of grade #4 after sputtering with deuterium plasma ions of the layer of ~1 μm.

No heterogeneities of this kind were found in the other two alloys: grade #2 and #5.

### 2.4. Plasma exposure and methods of surface analysis

To simulate the impact of charge-exchange atoms (CXA) flux on BMG mirror samples in ITER, ions of deuterium or argon plasma were used. The detail description of the experimental stand DSM-2 used for performing the ion bombardment can be found in [13,14]. The BMG mirror samples were exposed to electron cyclotron resonance plasma (ECR, frequency of generator 2.45 GHz) produced in a double-mirror magnetic configuration. Mirror specimens were fixed on a water-cooled holder just outside of magnetic mirror. During the exposure, the temperature did not exceed 40°C. The electron density of plasma was ~$10^{16}$ $m^{-3}$ and electron temperature ~5 eV. A fixed negative voltage (in the range 50–1350 V) was supplied to the mirror holder for the acceleration of ions to the mirror surface. In some cases, when using deuterium plasma, the ion flux was energy distributed between 50 eV and 1350 eV by the combination of fixed negative potential and a time-varying (frequency 50 Hz) half-wave positive potential for ion acceleration [13,14]. The latter was done to be closer to real energy distribution of CXA flux, calculated for ITER [2]. The mean ion current density to the sample was of the order of 1 mA/$cm^2$, that is, ~$10^{20}$ ions/$m^2$.

http://dx.doi.org/10.5772/63885

In the low-energy ECR deuterium discharge, there are usually not only monoatomic ions ($\mathbf{D}^+$) but also molecular ions ($\mathbf{D_2}^+$ and $\mathbf{D_3}^+$) [15]. In proximity to the mirror surface, such polyatomic ions fall apart into atoms and monoatomic ions in such a way that their energy, acquired during passing the accelerating voltage, is divided equally between fragments. Thus, the surface of mirror is bombarded by particles of equal mass but different energies: *E*, *E*/2, and *E*/3, where *E* is the ion energy due to application of an accelerating voltage. With this peculiarity of plasma composition and sinusoidal time variation of accelerating voltage, the character of calculated energy distribution of projectiles bombarding the mirror surface is in a qualitative accordance with the CXA energy distributions measured at tokamaks ([16, 17]) and calculated for ITER conditions [2].

All samples were exposed in several steps in DSM-2 to nonmass-separated plasma ions in order to study the evolution of investigated properties with fluence. After each exposure step, the mass change and the reflectance at normal incidence of light (range 220–650 nm) were measured. The state of sample surface was analyzed by various microscopes (in addition to mentioned SEM with EDX): optical microscope, interferometer microscope, confocal laser scanning microscopy (CLSM), atomic force microscopy (AFM); for some BMG samples, the state of surface was studied by secondary ion mass spectrometry (SIMS), electron microprobe method, and laser ablation method.

## 3. Properties after plasma exposure

### 3.1. Absorption of deuterium

#### *3.1.1. Amorphous specimens*

It was found that mirror samples of all grades absorb large amounts of deuterium after the mirror specimens were bombarded with ions of the deuterium plasma. Because of deuterium absorption, a weight gain was observed for all tested BMG grades, even if sometime clearly sputter erosion takes place. This is expected due to the high fraction of hydride forming elements (Zr, Ti, Be). In **Table 3**, the weight gain after each plasma exposure step for a sample of grade #1 is shown. For low enough energies, that is, up to 100 eV, one may suppose that ion sputter erosion is negligible. Therefore, the ratio of retained deuterium to the impacting ions can be calculated up to 100 eV, and is shown in **Figure 7**. Because the ECR discharge does not only produce $D^+$, but also $D_2^+$ and $D_3^+$ ions, the total flux of deuterium projectiles has to be somewhat larger than the ion flux measured, and, correspondingly, the portion of retained deuterium to impacting D atoms has to be noticeably lower, assumed within a factor of ~2.

The set of data for deuterium trapping by different samples is shown in **Figure 8**. The ion energy was fixed at 60 eV for the samples of grades #1 and #2, and at 100 eV for both sides of sample of grade #5, while it was increased from 30 to 600 eV for the sample of grade #4. Obviously, for fixed ion energy the deuterium uptake increases linearly with ion fluence.

| No of exposure step | Accelerating voltage, V | Ion fluence, $10^{23}$ ions/m$^2$ | Current density, mA/cm$^2$ | Weight change, μg/cm$^2$ | Absorption, D/ion, % |
|---|---|---|---|---|---|
| 1 | −30 | 8.1 | 1.2 | +21 | 7.7 |
| 2 | −30 | 8.1 | 1.2 | +18.4 | 6.8 |
| 3 | −1000 | 2.0 | 2.6 | 0 | ? |
| 4 | −20 | 8.1 | 1.2 | +26.3 | 9.7 |
| 5 | −100 | 9.2 | 1.37 | +69.7 | 22.6 |
| 6 | −60 | 9.2 | 1.36 | +48.7 | 15.8 |
| 7 | −60 | 9.8 | 1.54 | +35.5 | 11.7 |

**Table 3.** Results of sequential exposures of one sample of grade #1 in deuterium plasma.

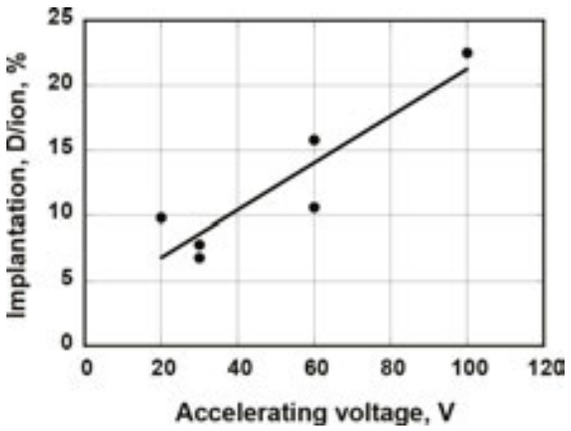


**Figure 7.** Dependence on ion energy of the portion of deuterium (in comparison to deuterium ion fluence) retained in the amorphous mirror sample of grade #1 [10].

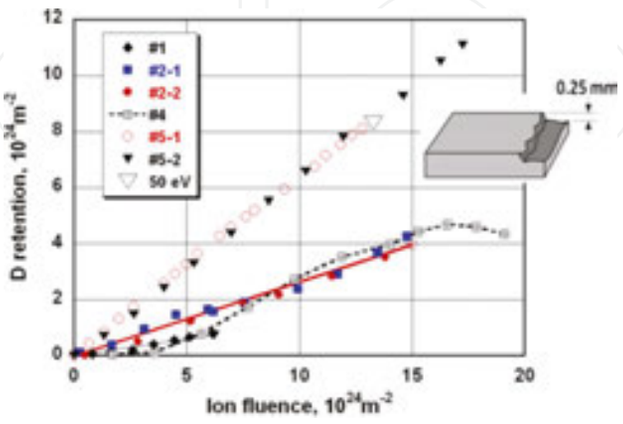


**Figure 8.** Dependence of deuterium retention for BMG samples on ion fluence found by measuring weight gain. The details are in the text. Inserted is the sketch of the sample of grade #5 after finishing its exposure in deuterium plasma on both sides. The chipped side was exposed secondly (triangles, #5-2) to the fluence $1.7\times10^{25}$ ions/m$^2$.

http://dx.doi.org/10.5772/63885

A very low level of absorbed deuterium for the sample of grade #4 at the lowest fluences (30 and 60 eV) is most likely explained by insufficient cleaning of this particular sample. A clear linear dependence takes place from 60 eV up to 150 eV (fluence range from (3.6–12)×$10^{24}$ ions/$m^2$), then sputtering starts to play more and more important role with increasing ion energy: at ion accelerating voltage of 400 V, sputtering and absorption are about equal, but with further rise of ion energy the weight started to decrease showing that sputtering prevails over deuterium absorption. An abrupt transition from linear dependence to saturation gives chance to estimate the thickness of sputtered layer, as it is described below (Section 3.2).

After last exposure in deuterium plasma (ion fluence~1.9×$10^{25}$ ions/$m^2$) the #4 grade sample became curved with radius of curvature ~24 cm in such a way that the side exposed to D plasma ions became convex.

The experiment with exposing front side of sample of grade #5 (data #5-1) was also stopped (at ion fluence 12.8×$10^{24}$ ions/$m^2$) after its bending was discovered, again with exposed side to be convex (curvature radius ~28 cm).

This fact indicates appearance of tension due to an increase in the specific volume of the near-surface layer exposed with deuterium plasma ions. The fact of bending means that deuterium does not penetrate through the whole thickness of samples, and only near-surface layer, of thickness less than the total thickness of sample, is increasing in volume.

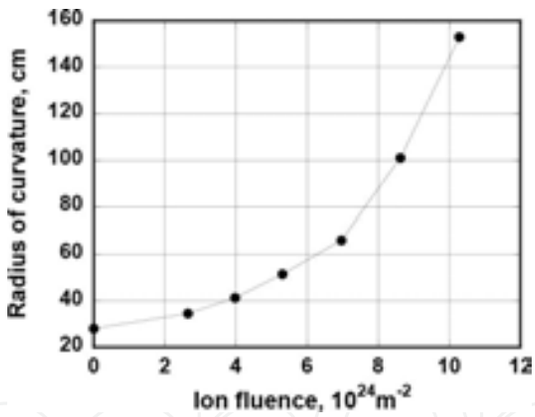


**Figure 9.** Straightening of the sample of grade #5 by exposing to the backside (#5-2 in **Figure 8**).

It was decided to continue the experiments by exposing the back side of the #5 sample in similar conditions (data #5-2 in **Figure 8**). During sequential exposures, the sample started to straighten gradually (**Figure 9**) and became plane at ion fluence ~12.0×$10^{24}$ ions/$m^2$, that is, after approximately the same fluence to the front side caused bending of the sample. Three further exposures resulted in beginning to bend the sample in opposite direction (radius of curvature ~100 cm) and its partial destruction. Schematically, the shape of the sample after full cessation of experiment is shown as insert in **Figure 8**. The thickness of the chipped off part is ~0.25 mm. Assuming the formation of zirconium hydride in δ-phase ($ZrD_{\sim 1.5}$) by all retained deuterium, the thickness of hydride layer would be 0.22 mm. This is excellent agreement with the observed thickness of the chipped fragment.

In **Table 4**, the efficiency of deuterium absorption is shown as the ratio of retained D atoms to the whole fluence of ions, found as the product of measured ion saturation current and the total exposure time, because the real proportion between one-, two-, and tree-atomic ions is not known (see comments in Section 2.3). It follows from **Table 4** that the efficiency of uptake depends strongly on ion energy and composition, but even with identical composition difference is significant (for grades #1 and #2).

| **Samples** | **#1** | **#2** | **#4** | **#5** |
|---|---|---|---|---|
| Ion energy, eV | 60 | 60 | 60–150 | 100 |
| Ion fluence, $10^{24}$ions/m$^{-2}$($F_i$) | 6.26 | 15 | 15 | 12.8 |
| Mass gain, mg/cm$^2$ | 0.27 | 1.33 | 1.5 | 2.71 |
| $N_D$ absorbed, 1024 D atoms/m$^{-2}$ | 0.8 | 4 | 5 | 8.1 |
| Efficiency of absorption ($N_D/F_i$ ) | 0.13 | 0.27 | 0.33 | 0.63 |
| Portion of Zr in composition | 41.2 | 41.2 | 48 | 57 |

**Table 4.** Comparison of deuterium uptake by different BMG samples.

Comparing data of the table, it looks like there is a tendency for efficiency of uptake to increase with increasing the portion of zirconium.

A laser ablation technique was applied as an attempt to see the depth distribution of trapped deuterium. The diameter of laser spot was ~0.3 μm, and the step in depth for every laser shot was ~1.5 μm. As shown in **Figure 10**, deuterium is confidently registered even after the laser crater depth reached ~28 μm, However, in this method, the effect of side walls of the laser crater cannot be fully excluded, and therefore, any quantitative conclusion on the real depth distribution of implanted deuterium can only be done with a definite precaution.

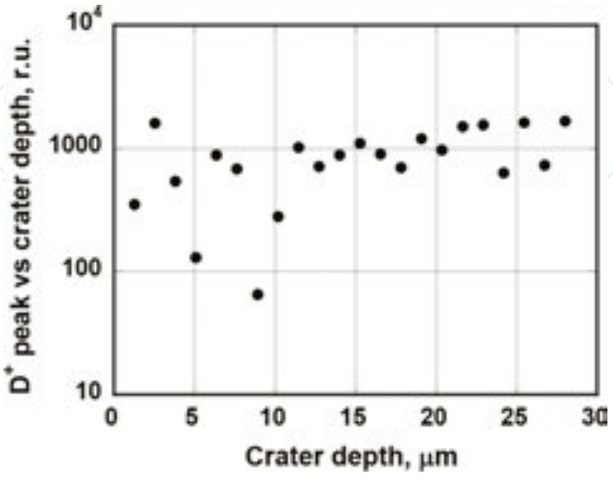


**Figure 10.** The amplitude of $D^+$ peak in ablated material as function of laser crater depth for a specimen of grade #1 exposed to deuterium plasma ions (60 eV/ion) up to a fluence of $5.9\times10^{24}$ ions/m$^2$.

http://dx.doi.org/10.5772/63885

Samples that were not exposed to deuterium plasma did not reveal a deuterium peak in their mass spectra, as can be seen in **Figure 11**. The hydrogen peak was registered in every spectrum; however, it is well known that such peak can be an artifact appearing due to not perfect vacuum conditions in the mass spectrometer chamber.

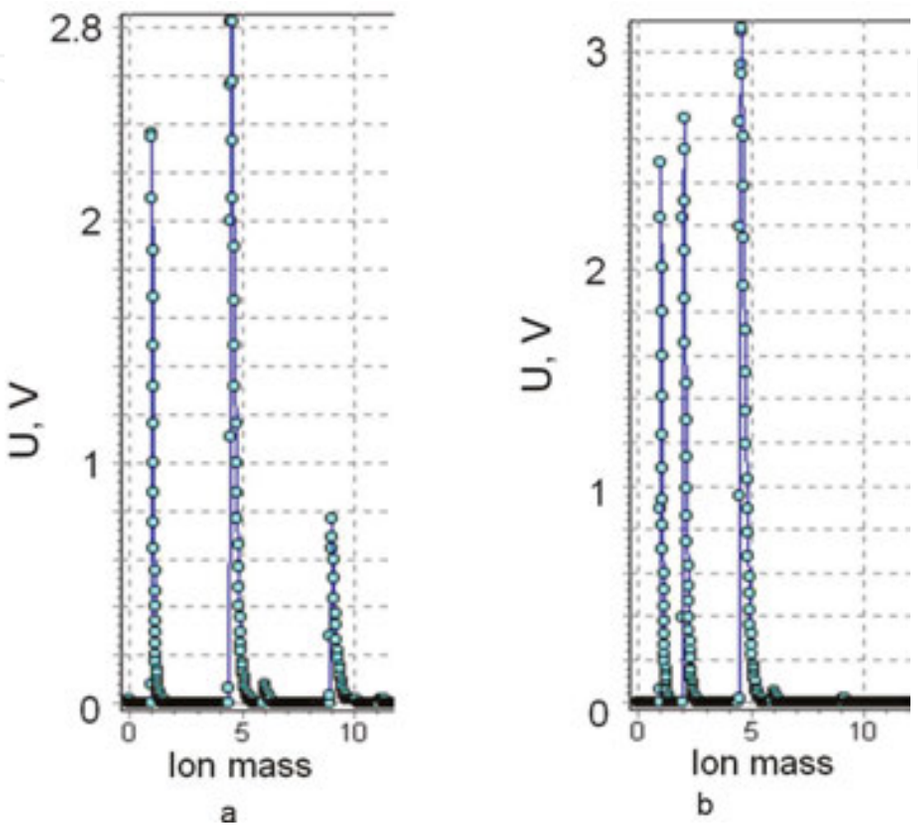


**Figure 11.** Mass spectra of the lighter masses of ablated material for samples of grade #1: (a) not exposed in plasma and (b) after exposure to deuterium plasma up to ion fluence $1.4\times10^{25}$ ions/m$^2$ with different ion energy. Peaks of ions $H^+$, $D^+$, $Be^{2+}$, $C^{2+}$, and $Be^+$ can be clearly distinguished [9].

For another sample of grade #1 exposed to a total ion fluence of ~$6\times10^{24}$ m$^{-2}$, a second laser ablation test was carried out 26 days after the exposure. During that time, the sample was stored at ambient atmospheric conditions. This sample showed a very different depth distribution, namely deuterium was not registered during first five shots, and then $D^+$ peak appeared in the sixth shot, reached maximal amplitude in the 7th shot and gradually decayed to zero in the 11th laser shot. However, the weight of the sample did not change, and thus, it may be assumed that the retained deuterium was redistributed inside the sample or that some of the retained deuterium was released, but the associated weight loss was balanced out by oxidation.

### *3.1.2. Crystallized specimens*

Two samples of grade #2, one amorphous (BMG) and one crystallized (BMG-C), were exposed in similar conditions for a long term to low-energy (60 eV) ions of deuterium plasma with a

current density of 2.1 mA/cm$^2$. Other important details of the experiment are presented in **Table 5**. During the fourth exposure (total ion fluence 7.5×10$^{24}$ ions/m$^2$), the BMG-C was fragmented, as shown in **Figure 12a**. On the contrary, its amorphous counterpart maintained its integrity and continued to gain weight during the following three exposure steps (total ion fluence 1.4×10$^{25}$ ions/m$^2$). The reflectance did not appear to be affected noticeably (not shown).

| No of exposure | Ion fluence, 10$^{25}$ ions/m$^2$ | Weight gain for BMG, μg | Weight gain for BMG-C, μg |
|---|---|---|---|
| 1 | 0.47 | 30 | 40 |
| 2 | 2.4 | 620 | 0 |
| 3 | 2.4 | 920 | 640 |
| 4 | 2.4 | 820 | Destroyed |
| 5 | 1.6 | 375 | |
| 6 | 2.4 | 825 | |
| 7 | 2.4 | 870 | |

**Table 5.** The history of weight change during exposure of samples of grade #2 to ions of deuterium plasma of 60 eV/ion, ion current density 2.1 mA/cm$^2$.

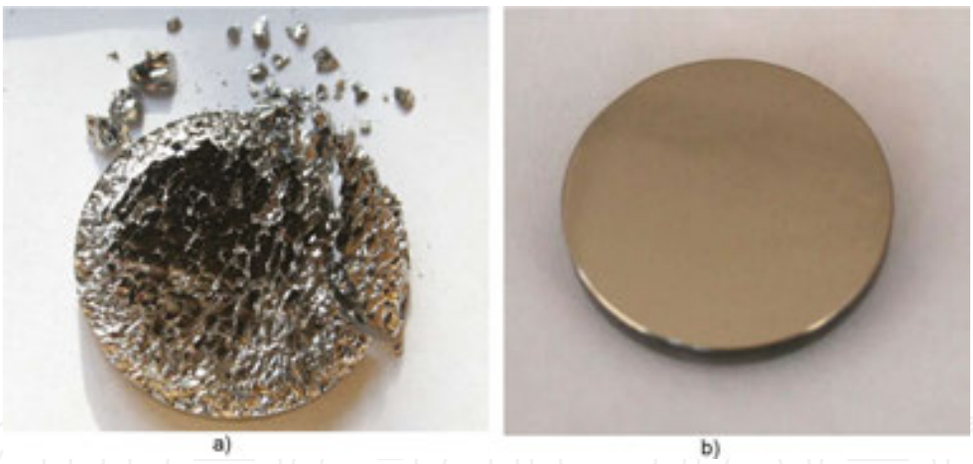


**Figure 12.** Photographs of (a) the BMG-C crystallized sample of grade #2 after the fourth exposure to 60 eV ions of deuterium plasma and (b) its amorphous counterpart (BMG) after the seventh exposure to 60 eV ions of deuterium plasma [18].

Not catastrophic for the sample, but detrimental for the optical characteristics was the modification of the surface of another crystallized mirror samples of grade #2, exposed to deuterium plasma ions in different regimes, **Table 6**. After the last exposure on the surface of this sample, there appeared defects in the form of chips and cracks of different sizes and significant weight loss was measured due to the loss of some fragments inside the vacuum chamber. The SEM images of chip surface at two magnifications, presented in **Figure 13**, exhibit the characteristic for a brittle rupture. The amorphous counterpart was unaltered.

http://dx.doi.org/10.5772/63885

Such difference in behavior of BMG and BMG-C samples is in a good qualitative agreement with the results published by Suh and Asoka Kumar on amorphous and crystallized samples of similar composition that were subjected to cathodic charging [19]. After a critical charging time, both amorphous and crystalline samples disintegrated. However, the maximum hydrogen content before total disintegration was up to 30 times greater for the amorphous phase compared to the crystalline counterpart.

| No of exposure | Working gas | Ion energy | Current density, mA/cm$^2$ | Ion fluence, $10^{23}$ ions/m$^2$ | Mass loss, μg |
|---|---|---|---|---|---|
| 1 | Ar | 200 eV | 1.4 | 3.2 | 1970 |
| 2 | Ar | 500 eV | 1.3 | 0.73 | 1195 |
| 3 | Ar | 1000 eV | 1.9 | 0 .36 | 980 |
| 4 | $D_2$ | 1000 eV | 2.1 | 1.6 | 0 |
| 5 | $D_2$ | 1000 eV | 2.1 | 2.4 | 20 |
| 6 | $D_2$ | 1000 eV | 2.1 | 2.4 | 130 |
| 7 | $D_2$ | 1000 eV | 2.1 | 2.4 | 560 |
| 8 | $D_2$ | 1000 eV | 2.1 | 3.2 | 265 |
| 9 | $D_2$ | 60 eV | 2.1 | 14.1 | 2900 |

**Table 6.** The history of exposure of one of the BMG-C crystallized samples of grade #2 to ions of argon and deuterium plasma.

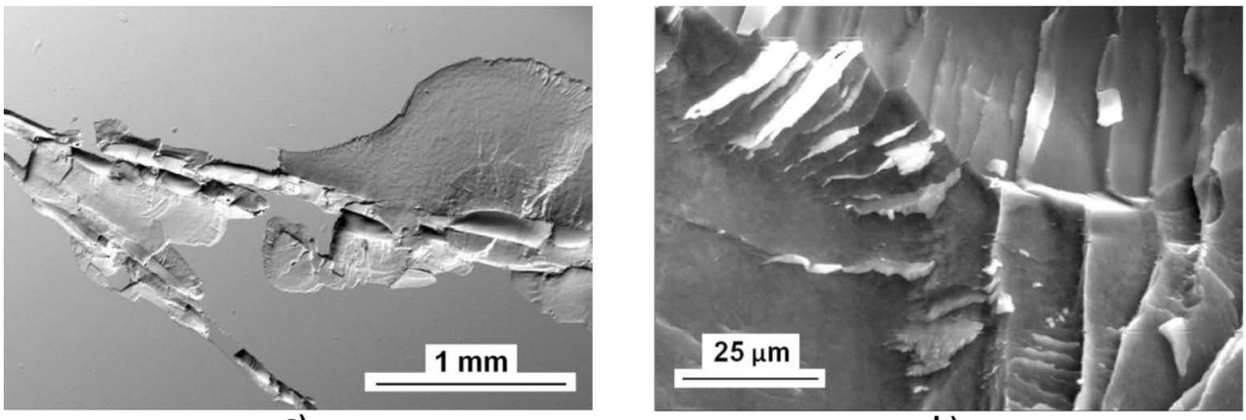


**Figure 13.** SEM images of the crystallized sample of grade #2 after the last exposure (no 9) shown in **Table 6** [18].

### 3.2. Sputtering rate

The adsorption of deuterium makes difficulties when trying to obtain data on sputtering yield by measuring the weight loss. Therefore, a stainless steel diaphragm (diameter 8 mm) which hid the rest part of BMG sample surface of grade #1 (diameter 22 mm) was used for determi-

nation of the rate of sputtering by deuterium plasma ions. The depth of the erosion hole measured for ion energies 300, 650, 1000, and 1350 eV are presented in **Table 7**. The corresponding values of sputtering yield were estimated with taking into account the depth of the hole, ion current density, and exposure time. The results are presented in **Figure 14**.

| No. of experiment | Ion energy, eV | Depth of erosion, nm | Microhardness, kg/mm$^2$ | Mass change, μg | k | n |
|---|---|---|---|---|---|---|
| 1 | 1350 | 709 | 639 ± 23 | -210 | 2.65 | 2.05 |
| 2 | 1000 | 660 | 621 ± 21 | | 2.69 | 1.91 |
| 3 | 650 | 505 | 668 ± 10 | +40 | 2.7 | 1.96 |
| 4 | 300 | 188 | 682 ± 18 | +80 | 2.68 | 1.93 |
| 5 | Not sputter eroded surface | | 540 ± 18 | | 2.61 | 1.77 |

**Table 7.** Results of exposure through a diaphragm (8 mm in diameter) of the sample of grade #1 for four ion accelerating voltage.

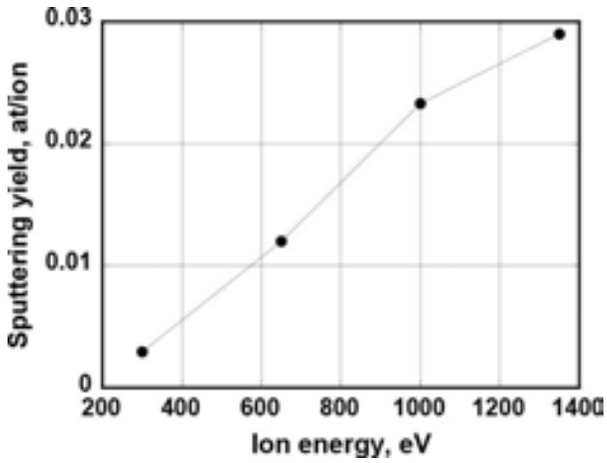


**Figure 14.** Sputtering yield found from the depths of holes appeared on the surface of sample of grade #1 exposed to $D^+$ plasma ions through an 8 mm diaphragm.

In addition to the erosion depth, the microhardness and the optical constants of surface inside each exposure spot were determined. It is seen from the **Table 7** that $D^+$ ion bombardment modifies the hardness of the near surface layer. The limited information on this subject, like the amount of trapped deuterium, its depth distribution, etc., does not allow to make a definite conclusion on the reason of this phenomenon, for example, on its link with volumetric density of trapped deuterium, as was found by the authors of [19].

After finishing the exposure to ions of energies indicated in the **Table 7**, optical indices *n* and *k* were measured with ellipsometry. **Table 7** shows that both optical indices do not depend strongly on the chosen $D^+$ ion energies and fluences; however, they differ a little from the indices measured for the initial surface, that is, not eroded by ions of deuterium plasma due to protection by diaphragm.

http://dx.doi.org/10.5772/63885

Because of the small size (Ø5 mm in diameter) of grade #3 samples the deuterium adsorption was not measured quantitatively for these samples (too low mass gain). Aiming to obtain data on sputtering, one sample of grade #3 was exposed to ions through a Ni gauze with wire diameter of 20 μm and mesh window width of 80 × 80 μm. The data obtained are shown in **Figures 15** and **16**. **Figure 15a** shows a typical photograph made with an interference microscope of the sample of grade #3 after it was bombarded with deuterium plasma ions ($E_i$=1000 eV, total ion fluence ~$6\times10^{24}$ ions/m$^2$) through the gauze, and **Figure 15b** shows the result of processing of the interference picture along several windows between wires of the gauze. As one can see, the sputter depth is about 1 μm. This depth corresponds to the sputtering yield (for not mass separated deuterium ion flux) $Y$≈0.05 atom/ion, which is about a factor two of the value found for grade #2 (**Figure 14**).

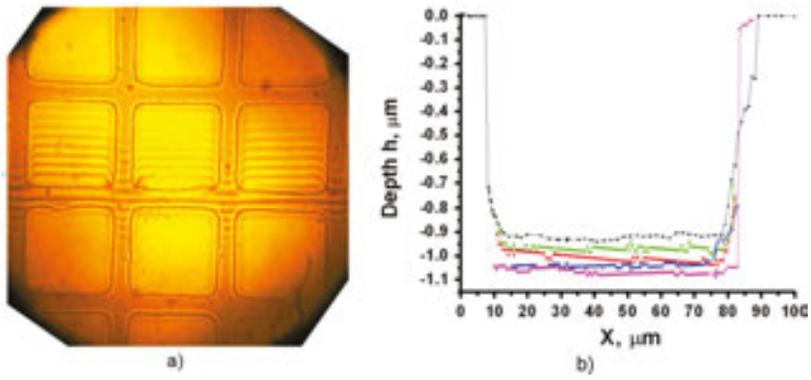


**Figure 15.** Interference fringes on the surface of the sample of grade #3 after long-term bombardment through the mesh (a), and the structure of the relief found by processing of the interference fringes (b) [20].

The optical and AFM data presented in **Figure 15** and **Figure 16** demonstrate similar depth of erosion in different windows. Also, they do clearly indicate that sputtering of the wire itself occurs because the edges of each wire are bombarded by ions at small angle to the surface, for which the sputtering yield exceed considerable the yield at normal incidence [21].

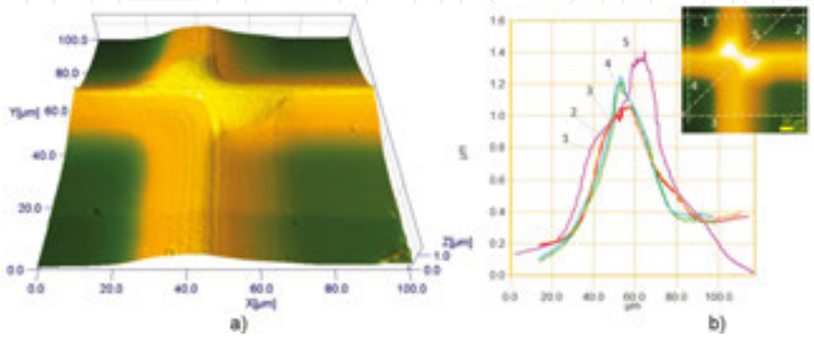


**Figure 16.** AFM data for the same sample of grade #3 exposed to plasma through Ni gauze as in **Figure 15**: (a) 3-D picture near crossing of Ni wires, (b) 2D picture of same data and height distributions along the lines shown in picture.

Important to note that saturation seen for the grade #4 sample in **Figure 8** is not because cessation of D absorption but due to faster mass loss caused by ion sputtering in comparison with the mass gain due to deuterium implantation. Taking this into account and comparing the linear fit of deuterium absorption with the saturation level of mass rise measured, one can find for this sample that thickness of sputtered layer after last exposure shown in **Figure 8** is ~1 μm, mainly due to sputtering by ions in the range 300–600 eV.

With the use of Ar plasma ions, there was not any problem to measure the weight loss even after short exposure. The results of these measurements for amorphous and crystallized specimens of grade #2, depending on the ion energy, are presented in **Figure 17** in comparison with data (solid line) for the bombardment of zirconium with $Ar^+$ ions from [11]. As seen, there is no measurable dependence in the sputter rate for samples in different state. Besides, there is a trend for lower sputter erosion rate of both samples in comparison to zirconium. This is in qualitative agreement with data for stainless steel in [21], sputtering yield of which was less than sputtering yields of each component (Fe, Ni, Cr).

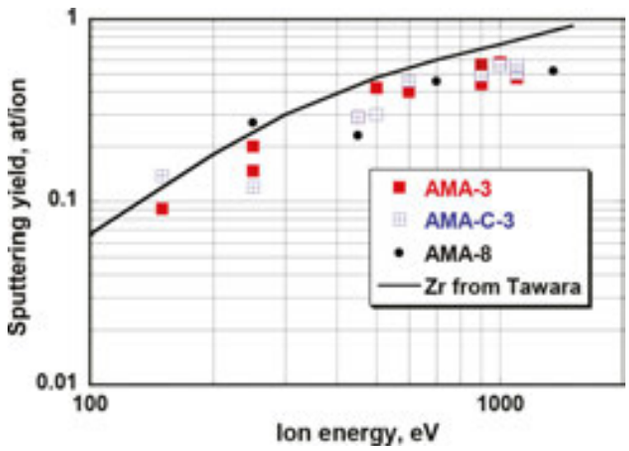


**Figure 17.** Sputtering yield depending on the $Ar^+$ ion energy for amorphous (BMG) and crystalline (BMG-C) mirror samples of grade #2. For comparison sputtering yield for pure Zr by Ar from Yamamura and Tawara [11] are shown. Amorphous sample BMG-3 and crystallized sample BMG-C-3 were made from same ingot.

When performing this experiment, not only mass loss but also the reflectance at normal incidence was measured after each sputtering procedure. Thus, the behavior of reflectance under long-term sputtering for samples (BMG and BMG-C) made from the same ingot of grade #2 but with different structure was determined (see next section).

### 3.3. Modification of optical properties of amorphous mirrors

#### *3.3.1. Impact of deuterium plasma ions*

When exposing BMG specimens of grades #1 and #2 in deuterium plasma, it was found that even rather short-time bombardment with ions of keV energy range, when sputter erosion

http://dx.doi.org/10.5772/63885

could be neglected, leads to a measurable decrease of reflectance in the whole spectral interval of measurement, both for amorphous (BMG) and for crystallized (BMG-C) mirror samples. The decrement of reflectance change depends on the wavelength: the shorter the wavelength the deeper the drop. The reflectance may be restored by long-time exposure to low energy (~50 eV) ions of deuterium plasma; the restoration is full or partial, depending on the exposure time to low-energy ions. This means that the reflectance decrease due to keV ion energy impact is not connected with modification of the surface microrelief but with some chemical processes on the surface, like it was established earlier for Be and Al mirror samples [22, 23]. We shall discuss this fact below in a special section.

As an example, **Figure 18** demonstrates the results obtained on one of BMG-C samples of grade #2. Initially, it was sputtered with ions of Ar plasma, what resulted in the development of some surface roughness and corresponding reflectance decrease (solid circles ⇒ squares). Then, the sample was bombarded with 1.0 keV ions of deuterium plasma, what caused further reflectance drop (rhombuses); however, not due to increase of the surface roughness, because this drop was fully restored by subsequent (much longer) exposure to low-energy (60 eV) ions of the same deuterium plasma (open circles). In contrast, the drop of reflectance caused by Ar ion sputtering could not be restored in similar way, that is, by exposing sample to low energy $D^+$ ions, as it occurred due to development of surface roughness.

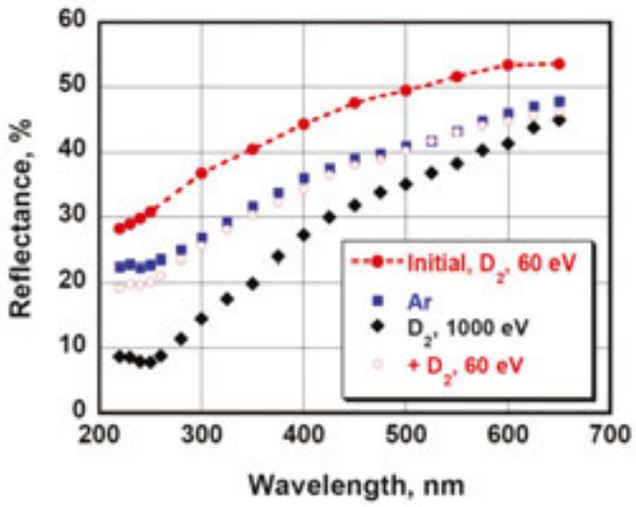


**Figure 18.** Spectral dependence of reflectance for BMG-C mirror sample of grade #2 after short exposure (ion fluence of the order $10^{22}$ ions/m$^2$) to ions of deuterium plasma with energy 1 keV (◆) and following much longer exposure to 60 eV deuterium plasma ions (o).

The correlation of drop and restoration of reflectance for Be-containing BMG samples of grade #2 is in qualitative agreement with the results of experiments when specimen of grade #1 was exposed by turns to high (1.0 keV) and low (60 eV) energy ions of deuterium plasma [10].

For BMG specimens of grade #3, qualitatively similar effect was observed; however, detail investigation was not provided because of small size (diameter 5 mm).

*3.3.2. Impact of argon plasma ions*

To avoid the effects connected with chemistry, the consequence of long-term erosion was studied by the use of Ar plasma ions. In comparison with deuterium, the use of argon as a working gas is characterized by the following three principle moments: (1) argon is inert under most conditions and does not form confirmed stable compounds at room temperature; (2) argon uptake and the creation of a contaminating layer on the metal surface may be neglected; and (3) the time of experiments can be much shortened because of the sputtering rate of BMGs with $Ar^+$ ions is significantly higher as compared with $D^+$ ions.

The evolution of the microrelief and the reflectance of BMG mirror sample of grade #2 was determined up to erosion depth of 13.4 μm by sequential exposures to $Ar^+$ ions of different energy (0.1–1.35 keV). **Figure 19** shows the reflectance at three wavelengths versus the thickness of eroded layer. The data demonstrate that the amorphous mirror maintains the reflectance at about initial value even after strong sputter erosion. The constancy of reflectance means that the surface of amorphous mirror does not change during all sputtering procedures. This fact confirms the supposition made by Voitsenya et al. [5].

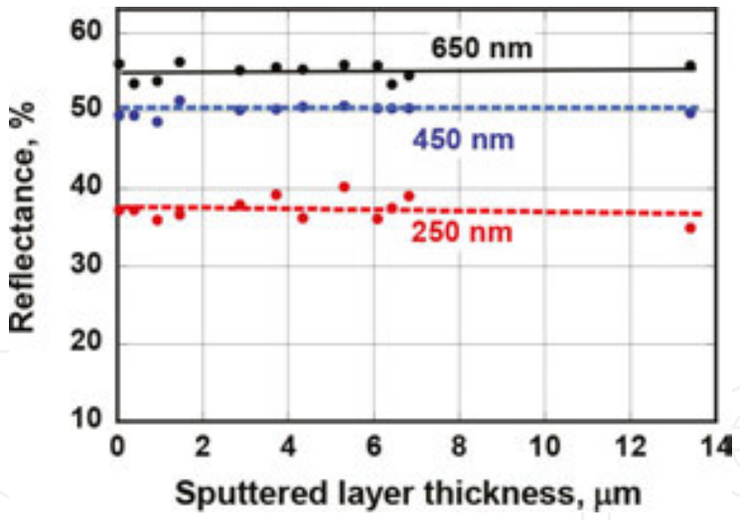


**Figure 19.** Dependence of reflectance of one of BMG sample mirrors of grade #2 on thickness of layer eroded due to manifold exposures to ions of Ar plasma with different energy [20].

At the same time, the surface of BMG-C sample (grade #2) made from same ingot but crystallized, became quite rough after sputtering to much lower erosion depth. In **Figure 20**, the comparison of SEM images of both samples are shown at the same magnification. One can observe that the relief appeared on the surface of the crystallized sample of grade #2 has approximately the lateral size of ~1 μm, while the amorphous sample of grade #2 stays very smooth.

http://dx.doi.org/10.5772/63885

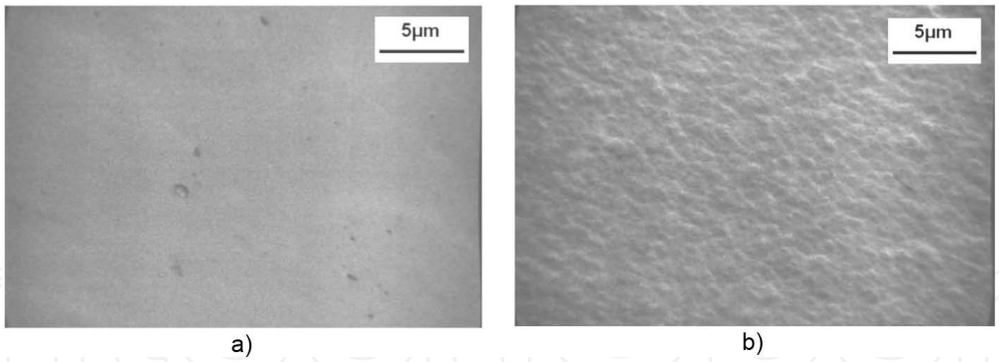


**Figure 20.** SEM photos of (a) BMG and (b) BMG-C specimens of grade #2 (made from the same ingot) after sputtering by Ar plasma ions to the depth 13.4 μm and 8.9 μm, respectively [10].

We have to emphasize a very significant difference in behavior of optical characteristics of mirror samples of grade #2 with amorphous (BMG) and crystalline (BMG-C) structures. The development of roughness on the surface of BMG-C (**Figure 20**) resulted in degradation of its ability to transmit an image. **Figure 21** shows the images of He-Ne laser beam spot after reflection: (a) from etalon mirror (Al film on quartz, that is, "ideal mirror"); (b) from amorphous mirror of grade #2 after long-term bombarded with $Ar^+$ ions (13.4 μm sputtered); and (c) from crystallized BMG-C sample of same grade after Ar bombardment (8.9 μm sputtered). The reflection of the crystallized BMG-C is strongly distorted, while the image of the eroded BMG has about the same quality as that from the "ideal mirror". The results of comparative analysis obtained when processing these images are presented in Appendix B.

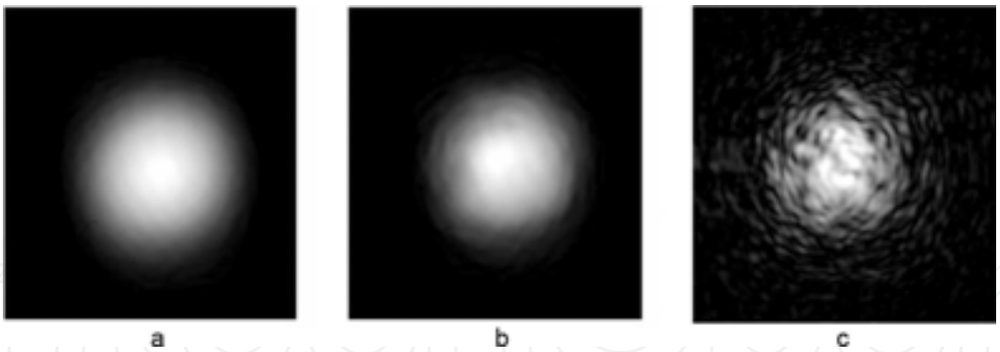


**Figure 21.** Image of the Ne–He laser beam spot after the beam was reflected from (a) "ideal mirror", (b) from sample of grade #2 after sputtering 13.4 μm, and (c) from crystallized sample of grade #2 after sputtering 8.9 μm [24].

### 3.4. Role of chemical processes

The qualitative similarity between behavior of reflectance of Be-containing BMG mirrors and Be mirrors exposed in similar manner suggests that in all cases similar processes are realized on the surface for mirror after impact of deuterium plasma ions with high (~1.0 keV) and low (~50 eV) energies. From the study of Bardamid et al [22], the reason of this transformation of BeO into $Be(OD)_2$ and gradual rise of hydroxide film thickness after the sample is subjected to

keV-energy ions of the plasma that contains also some amount of oxygen. An inverse process, namely restoration of initial state with thin BeO coating, on the Be surface occurs when ion energy is low.

To check this explanation, six BMG samples of grade #3 were sputter eroded by ions of Ar plasma to the depth of ~2 μm—for taking off the consequences of previous work with them. Then, four of them were bombarded by D plasma ions with energy of 1.35 keV. After that two of them were additionally long-term exposed to 60 eV ions of D plasma. SIMS analysis (with Cs+ ions as projectiles) was provided in two different points of the surface of the three pairs of samples. In connection with good equivalence of four data sets for each procedure (exposure to Ar ions, plus exposure to 1 keV D ions, plus exposure to 60 eV D ions), only results obtained from one point of one sample are shown in **Figure 22** for simplicity.

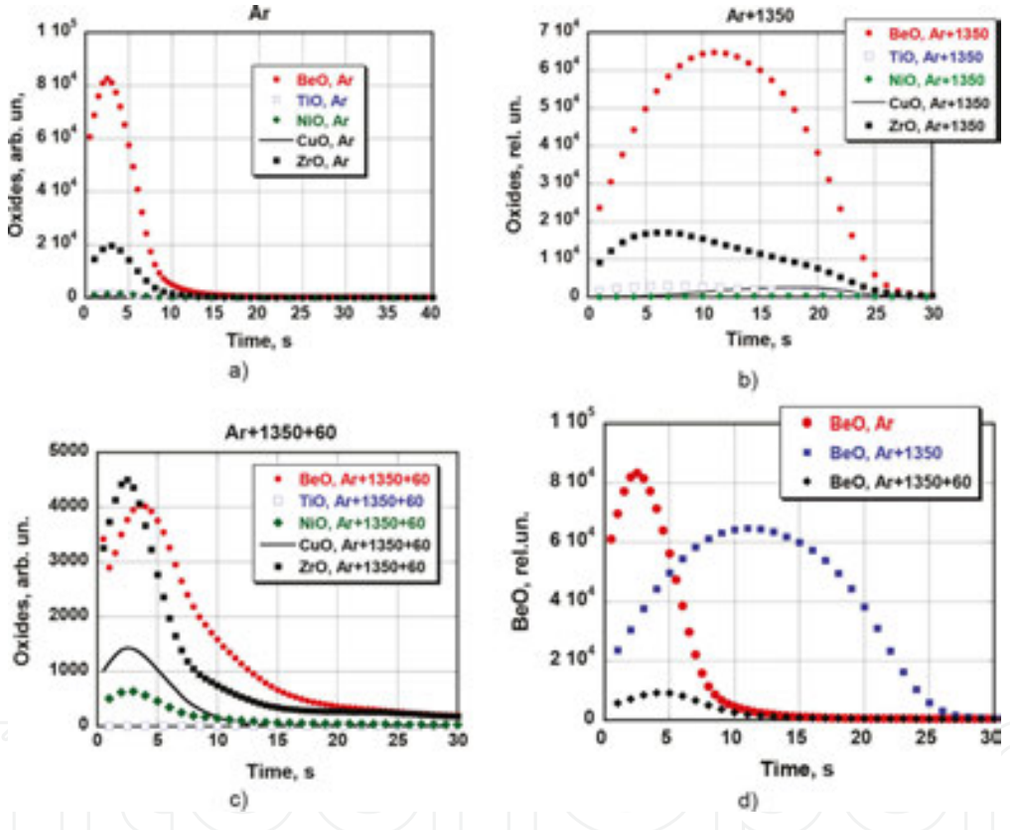


**Figure 22.** SIMS data for release of oxide ions for all components composed of BMG specimens of grade #3 after: (a) sputtering with Ar ions, (b) sputtering by Ar ions plus bombardment with 1.35 keV ions of deuterium plasma, (c) same as (b) plus long-term exposure to 60 eV ions of deuterium plasma; (d) comparison of the data for BeO ions only [18].

Evidently, the bombardment with keV-range D plasma ions leads to increasing the thickness of uppermost oxidized layer, but the following exposure to low-energy ions of similar D plasma results in thinning this layer and restoration of the initial depth distributions of all oxides.

These SIMS measurements were carried out with specimens having only 27.5 at.% of beryllium. At the same time, the release of $BeO^+$ ions significantly exceeds the release of all other oxides

http://dx.doi.org/10.5772/63885

together. However, because the relative sensitivities of the various oxides in the SIMS measurements are unknown, no conclusion about depth distribution of different oxides in the near-surface layer can be obtained. It is worth to add that SIMS results are in qualitative agreement with data of XPS (X-ray photoelectron spectroscopy) measurements on specimens with a similar composition [25]. The authors of that paper have found that the uppermost oxide film is mainly composed of BeO in spite of a quite complicated chemical composition of the material.

Similar chemical processes are probably responsible for different ratios of $Be^{+}$ and $Be^{2+}$ peaks shown in **Figure 11** when comparing the output at laser ablation of different ions from BMG samples of grade #1 exposed and not exposed to ions of deuterium plasma.

It is worth to note that qualitatively similar effects on the reflectance (drop for keV ion energy range and restoration for low-energy ions) were observed also for BMG samples of Al-containing grades #4 and #5, although not so strong.

### 3.5. Blisters

After the determination of sputtering rate by D plasma ions (Section 3.2), many small surface features were found in that part of one BMG mirror specimens (22 mm in diameter) of grade #1 which was exposed to ions with energy 300 eV (diameter of diaphragm 8 mm, ion fluence $2.4\times10^{24}$ ions/m$^2$). These "blister-like" features covered approximately 15% of the irradiated surface and generally had a round shape **Figure 23a**. Their size distribution (diameter) was obtained by measuring the dimensions of 617 such subjects observed in the view field of the microscope, ~0.4 mm$^2$. The mean diameter was ~10.5 μm with sizes ranging from ~3 up to 60 μm (one subject). The size distribution of these subjects is shown in **Figure 23b**. In the following sections, we use the word "blisters" for these subjects, in spite they do not look like a "classical" blisters, described by Behrisch [27].

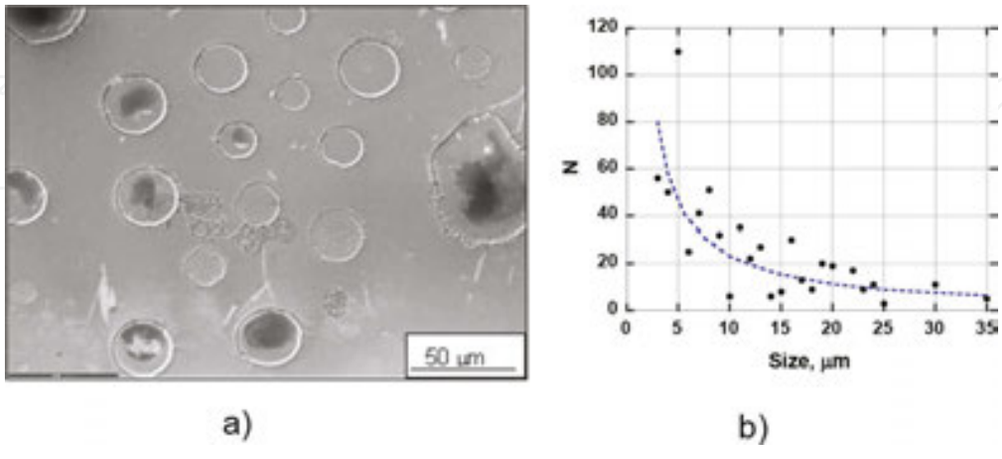


**Figure 23.** (a) SEM photo of the BMG mirror surface of grade #1 from secondary electrons with characteristic surface features [26]. The rough parts seen a little below the center are the structure defects described in the part 2.2 (see **Figures 3** and **4**); (b) size distribution of blister.

**Figure 24** shows atomic force microscope (AFM) images of the two different types of blisters and **Figure 25** – the corresponding cross-section profiles. The height of the flat-top blister (**Figure 24a**) is ~0.2 μm and it is surrounded by an annular groove of approximately similar depth. The blister of similar size, but with a black central area (**Figure 23**) can be seen in **Figures 24b** and **25b**). This time, there is an irregular-shaped dome on a flat lid base; the dome is seen as black color in **Figure 23a**.

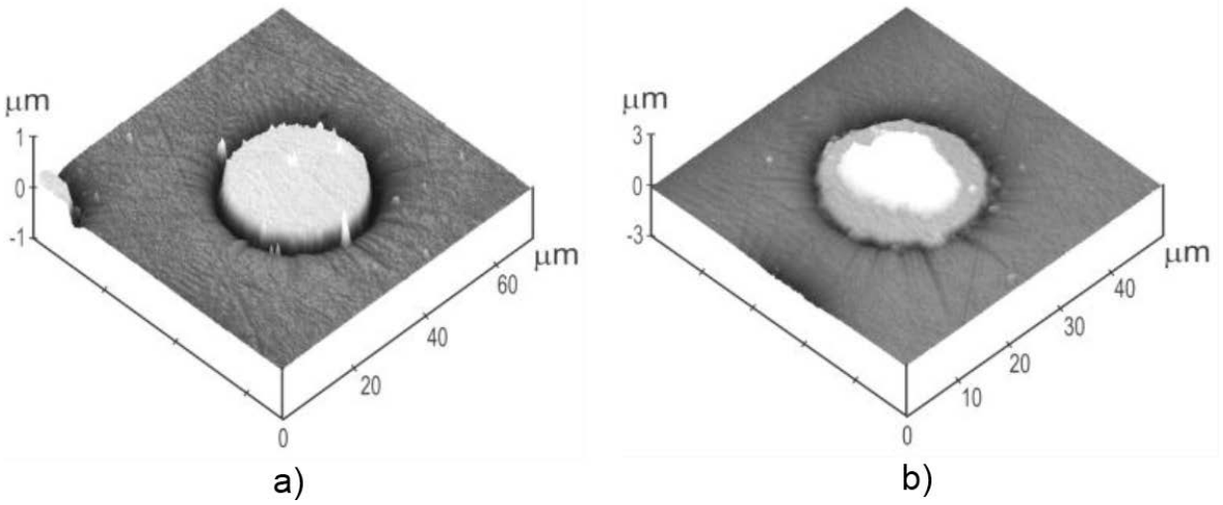


**Figure 24.** The AFM images of two different kinds of blisters: (a) with flat lid and (b) with a dome-like lid [26].

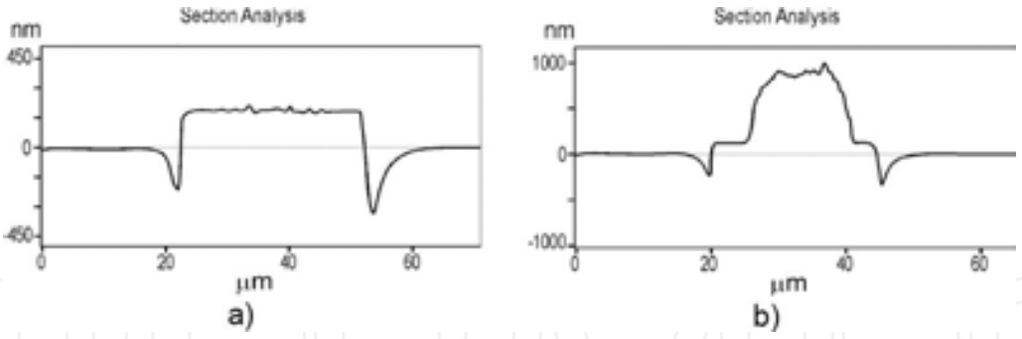


**Figure 25.** Cross-sectional profiles of the blisters shown in **Figure 24** [26].

A small part of the blisters is not round, and some of them have a dark part localized closer to their edge. Elemental maps obtained by EDX suggest that the elemental composition of the dome differs from that of the main BMG matrix.

The elemental composition of blister surfaces was obtained by two methods: microprobe analysis and EDX. On blisters with a uniform contrast and smooth lid, there was not found any noticeable deviation of composition in comparison with the matrix. At the same time those blister lids without contrast uniformity, seen with BSE, showed presence of impurities. As an example, in **Figure 26**, EDX-maps are shown for one of such blisters on the sample of grade

http://dx.doi.org/10.5772/63885

#1. It is seen that in darkest part of the surface (BSE) there are elements that are not a part of BMG composition: for example, carbon, oxygen, and iron.

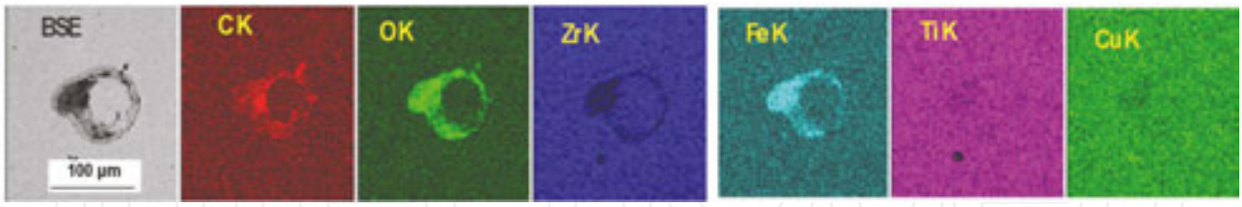


**Figure 26.** EDX-maps for a part of #1 sample surface with a large blister (~Ø65 μm).

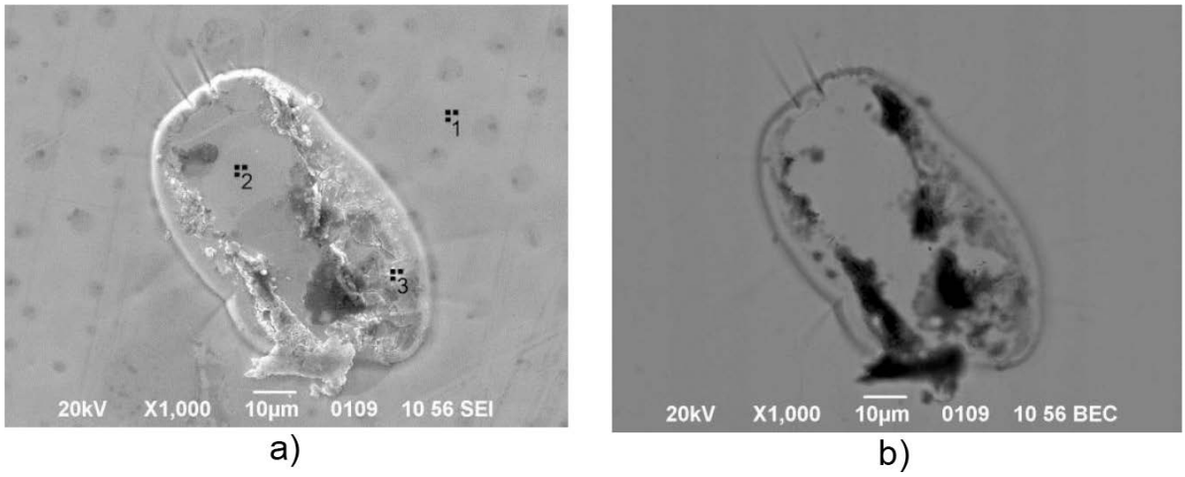


**Figure 27.** Image of a large blister with indication of points, P1 to P3, where measurements of composition were done: (a) SE and (b) compo (BSE).

In **Figure 27**, SE and BSE images of a blister on another sample of grade #1 are shown; the blister lid is not smooth partly. Numbers 1–3 indicate the points where a microprobe analysis was done (note that Be, C, and O cannot be registered by used setup). The results of measurements in those points are presented in the **Table 8**. Again, a small amount of impurity at the lid, this time, chromium, was registered. Based on results of EDX data for other blisters, one may assume that in the dark parts of the lid there are C and O also.

Several peculiarities of the blisters can be noted from presented data: (i) the blister location on the surface does not depend on the presence of defects in the grade #1 BMG described in the Section 2.3 (this is clearly demonstrated by **Figure 23a**); (ii) it looks like there is a probability that large blisters are localized in those parts where there are some concentration of contaminants, like iron, chromium, which can appear to be random; (iii) the parts of blister lids that look darker in BSE images are contaminated with carbon and oxygen; (iv) around practically every blister, there is evidence of stress-induced ductile deformation leading to a depression; (v) the inspection of several hundred features did not result in the observation of any cavity such as might be found following the bursting of blisters.

| Element | Passport data, at% | Matrix (P1), at.% | Smooth part of the blister surface (P2), at.% | Coarse part of the blister surface (P3), at.% |
|---|---|---|---|---|
| Zr | 41.2 | 56.6 | 57.7 | 49.7 |
| Ti | 13.8 | 16.9 | 17.3 | 15.4 |
| Cu | 12.5 | 13.9 | 13.1 | 12.4 |
| Ni | 10.0 | 12.1 | 12.0 | 11.7 |
| Hf | | 0.6 | | 0.6 |
| Fe | | | | 8.3 |
| Cr | | | | 1.9 |

**Table 8.** Results of microprobe analyses in points indicated in **Figure 27**.

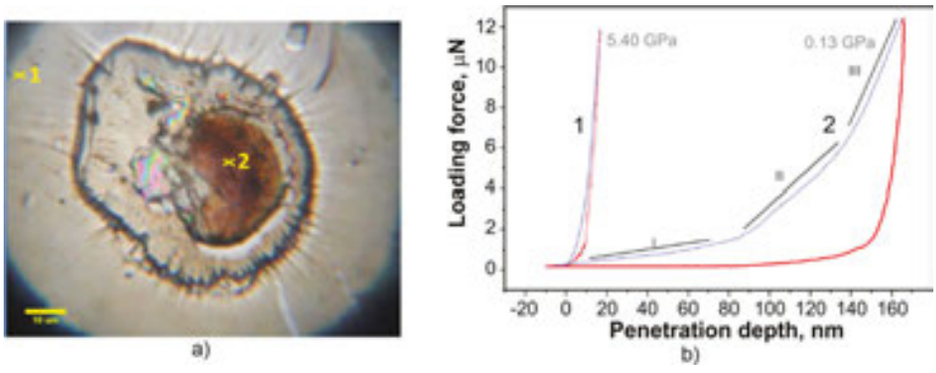


**Figure 28.** (a) Location of pricks by a nano-pin (yellow crosses) at the surface of a large dome-like blister, seen in **Figure 23a**. (b) The load and unloading curves of indenter measured at locations indicated in (a).

To clear up the reason of difference between both kinds of blisters, the nanoindentation procedures [28] were provided in matrix, in plane, and dome-like lids. The location of measurements is shown in **Figures 28a** and **29a**. The results are presented in **Figures 28b** and **29b**.

It is seen that the dark part of blister lid is soft and ductile. Three zones can be distinguished on the load curve: soft near-surface layer with ~80 nm in thickness (I), transition layer (II), and more solid material (comparable with hardness of matrix) at the depth starting from 140 nm (III).

These measurements demonstrate that the structure of the uppermost layer is very different for this pair of blisters: the dome-like one has a very soft uppermost layer (up to about 80 nm); the hardness of the material here became to be comparable with that measured for the plane-roof feature only at the depth ≥140 nm. At the same time, for plane roof feature, the hardness is much higher, composing ~60% of the matrix hardness.

http://dx.doi.org/10.5772/63885

Blisters were previously observed on metallic glasses of several kinds and on their crystal analogues after bombardment with $H^+$ and $He^+$ ions of energies up to 100 keV [29–31]. As was found, on amorphous materials blisters appear at ion fluences approximately three times greater than on the same materials in crystalline state. The blisters had dome-shaped lids with diameters in the range 0.5–2.5 μm (mean value 1.25 μm) for $H^+$ ions [29]. Such dimensions correlate well with the implantation range of the $H^+$ ions, thus suggesting the formation of "classical" blisters [27] due to accumulation of hydrogen in the near-surface region.

In conclusion, we would again state that difference in size, along with the atypical shape (like flat lids, annular grooves, the lack of broken lids, etc.), indicate that the observed features are not blisters in common understanding of this word [27].

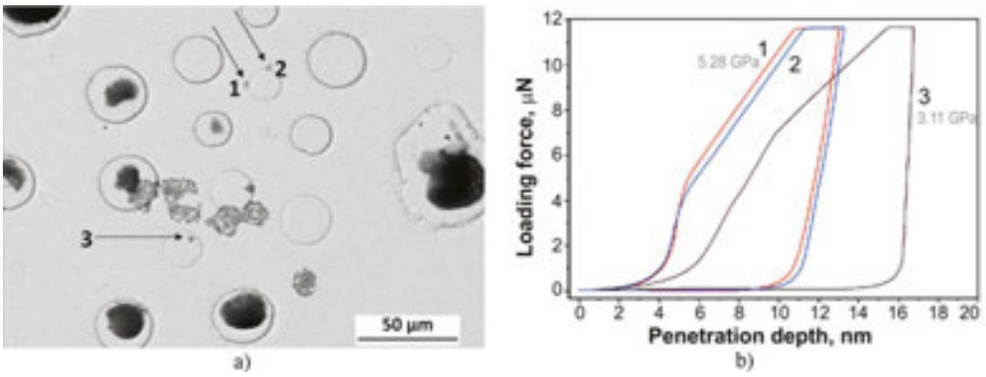


**Figure 29.** (a) SEM photo from backscattered electrons of the part of the surface shown in **Figure 23a**. (scale is 50 μm). Locations of pricks by a nano-pin at the surface of a plain lid blister and nearby matrix are shown by lower arrow and upper arrows, correspondingly. (b) The load and unloading curves of indenter measured at locations indicated in (a).

## 4. Summary

BMG mirror samples of different elemental composition were investigated in experiments simulating the behavior of first mirrors under impact of charge exchange atoms in the fusion reactor ITER. As projectiles the ions of deuterium and argon plasmas were used. Behavior of optical properties and surface topography, uptake of deuterium, effects of sputtering on optical reflectance in the visible spectrum, and chemical processes in a near-surface layer were studied. It was found that some of the studied properties have weak dependence on material composition whereas the others show noticeable differences. The following statements can be made:

1. Initial reflectance of BMG mirror samples under study is close to reflectance of W mirror for wavelengths exceeding 300-500 nm. The highest reflectance was measured for samples of grade #2 independently on the state: amorphous or crystallized.

2. In the body of three kinds of samples, structural inhomogeneities were described, which are connected with deviation of local composition from the composition of matrix, as was studied in detail for BMG samples of grade #1. The composition of inhomogeneities, that

occupied small part of the sample volume, was depleted with zirconium in comparison with amount of Zr on average. The ion-sputtering rate of material in these parts was higher than that of the main matrix, which leads to shallow depressions appearing on the sample surface with a rather planar bottom of 10–30 μm in size and the depth depended on sputtering time.

On the samples of grades #3 and #4 inhomogeneities of relief became clearly visible after eroding a layer exceeding 1 μm, either with ions of argon (grade #3) or deuterium plasma (grade #4).

3. Under long-term ion bombardment (thickness of sputter eroded layer was 13.4 μm in the case of #2 grade) no noticeable change of surface topography and reflectance for matrix of all BMG mirror samples was observed, excluding grade #4, where inhomogeneities occupied a rather big portion of the surface. In contrast, significant degradation of the mirror surface quality was found for the crystallized BMG sample of grade #2 sputtered to much less depth than its amorphous counterpart in similar conditions.

4. Under bombardment by deuterium plasma ions some amount of deuterium is absorbed, with the tendency to increase of absorbed portion when increasing the portion of zirconium. The highest value of deuterium was absorbed by BMG sample of grade #5: $1.1\times10^{25}$ D atoms/m$^2$.

   The absorbed deuterium, most likely, does not penetrate through the whole thickness of the sample but is accumulated in the layer with a thickness of a few tenths of millimeter (note, thickness of samples is 2–3 mm). At ion fluence exceeding $1\times10^{25}$ ions/m$^2$ samples become bent in such a way that the front side (exposed to ions of deuterium plasma) became convex with radius of curvature ~24 cm for grade #4 and ~28 cm for grade #5. Following exposures in similar conditions of the back side of grade #5 resulted in gradual straightening of the sample, and even bending it in opposite direction with further increase in ion fluence.

5. For samples of grade #2 in amorphous state, the deuterium ion fluence ($15\times10^{24}$ D ions/m$^2$) much exceeded the value for their crystallized counterparts when they started to the destroy: ~$5\times10^{24}$ D ions/m$^2$.

6. After implantation of deuterium (up to $1.1\times10^{25}$ D atoms/m$^2$ for grade #5 sample), there was not observed any indication on appearance of crystallized phase in amorphous samples.

7. There was not found any measurable effect of deuterium implantation on optical properties of mirror sample, either in amorphous or crystallized states.

8. On a small part of the surface of BMG mirror sample of grade #1, exposed to ions of deuterium plasma accelerated to the energy 300 eV, the blister-like features appeared with the shape different from what can be found in literature.

9. When BMG mirrors with beryllium or aluminum in their composition are exposed to deuterium plasma, chemical processes on the surface play a definite role in behavior of their optical properties.

http://dx.doi.org/10.5772/63885

In conclusion, we noted that because of the high absorptivity of hydrogen isotopes, existing Zr-based BMG cannot be a prospect material for in-vessel mirrors in ITER. However, in view of rather rapid progress in the development of amorphous materials, there is a hope that BMG materials with a low absorptive capacity (for hydrogen isotopes) will be designed in the future, what will permit their use for fabrication of in-vessel mirrors operating in the conditions with high fluxes of charge exchange atoms, neutrons, and gamma radiation.

## Acknowledgements

The authors would like to express their thanks to A.I. Belyaeva and O.A. Galuza, with whom some of presented results were obtained.

**Appendix A: Fabrication of amorphous alloys containing beryllium**

The main peculiarity of bulk amorphous metal alloys is that they have a multicomponent mixture; as the rule, 4–5 components are used for their preparation. Among the most perspective is Zr-based bulk amorphous metal alloy that demonstrate a high mechanical strength and fracture toughness with good corrosive resistance. For the system Zr-Ti-Cu-Ni-Be, the maximal critical thickness known from literature amounts to 30 mm at the critical cooling rate 1–5 K/s. This opens the way for preparation of mirror samples with a standard size (diameter 22 mm and thickness 3–4 mm) for experimental modeling the behavior of mirrors in ITER.

For smelting of ingots of bulk metallic glasses in Kharkov (grade #2, **Table 1**), an electric arc-smelting device with the nonconsumable electrode was used. The melting operation was realized in water-cooled copper mold, inside its cavity of reference shape and dimensions.

The alloy has the following composition: Zr41Ti14Cu12,5Ni10Be22.5. The purity of all metal components was not less than 99.9 weight percent. As the starting materials the iodide Zr and Ti, cathodic Ni, electrical copper, and distilled Be were used.

All components were mixed in the necessary proportion and placed in a mold cavity of the water-cooled copper mold of the melting facility. After that the melting facility was pumped for degassing the furnace charge and filled with pure argon to the pressure that ensures a stable arc burning. Then, arc was initiated and the metal got fused. The form and the size of ingots are specified by the mold cavity shape and amount of the furnace charge. For obtaining a homogeneous composition of an amorphous material it was molten many times with opening the melting facility and with flip over of the ingot for 180°. The initial sizes of ingots (diameter 25–28 mm and thickness 10–14 mm) were defined by the requirements to have the standard size of mirror samples (22 mm in diameter).

The billets for fabrication of mirror samples and specimens for providing different investigations of the properties of the amorphous material were prepared by means of electric discharge sawing. **Figure A1** shows the photos of one of ingots from which the upper and lower "caps" were cut off (left), before it was cut further into two halves (right) which served as billets for fabrication of mirror samples. One half of every ingot was annealed at 773°K during one hour.

The crystallization was checked by using the X-ray diffractometer DRON-4-07, and the results are shown in **Figure 1**.

**Figure A1.** The photos of the ingot with cut off upper and lower "caps" before (left) and after (right) cutting into two halves which served as billets for the fabrication of mirror samples.

## Appendix B: Processing of images of laser spots reflected from test mirrors

To study the structure of a laser spot image after laser beam reflection from a given surface, the sampling of brightness of pixels B(x) for every image in **Figure 21** was carried out along its diameter following a horizontal line or lines inclined at 45°, 90°, and 135° to this line. The spot is 440 pixels in diameter that corresponds to 4 mm. We removed a sampling component corresponding to a radial decrease in the spot brightness ("a bell shape") using a Fourier transform. The sequential combination of samplings extends the sampling path and improves the statistics.

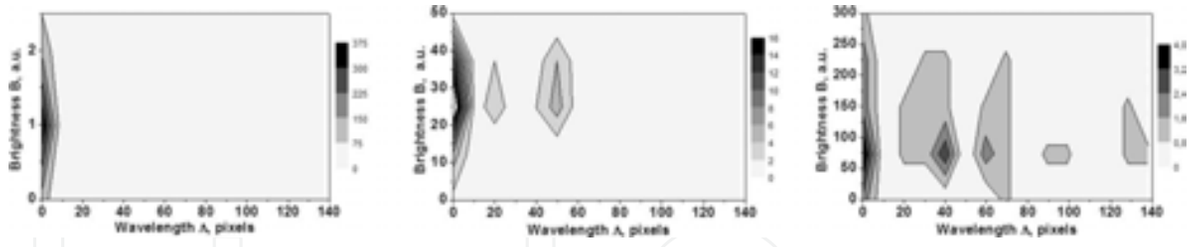


**Figure B1.** The contour diagrams of the distributions $\Delta N/(\Delta\Lambda \cdot \Delta B)$. The designations correspond to the laser spot images a–c of **Figure 21**.

A comparison of the samplings "by eye" shows that $B_a(x)$ is characterized by very short wavelengths and very low variations of the brightness. These parameters are higher for $B_b(x)$ and much higher for $B_c(x)$ by the reason of increasing the surface roughness.

The procedure described in [32] is intended to compute the one-dimensional distribution function $\Delta N(\Lambda)/\Delta\Lambda$ or, in other words, the number of waves N in a spectral interval $\Delta\Lambda$ where the wavelength $\Lambda$ is along the image. We extended this function to two-dimensional one $\Delta N(\Lambda,B)/(\Delta\Lambda \cdot \Delta B)$. The functions a–c are marked with constant-level lines in the contour diagram of **Figure B1**. The upper limits of the wavelength axis $\Lambda$ are the same for all the spots, and those of the brightness axis B are different.

We observed one group with the very short wavelengths and the very low oscillations of the brightness for the laser spot *"a"* (the "ideal mirror"). The spot *"b"* (BMG mirror) has three groups of the short and medium wavelengths, and the medium variations of the brightness. And the spot *"c"* (BMG-C mirror) has five groups of the short, medium, and long wavelengths, and the medium and high variations of the brightness. The results of an analysis are shown in **Table B1**.

| | $B_{av}$, a. u. | $B_s$, a. u. | $B_{max}$, a. u. | $S_m$, pixels | $\Lambda_{max}$, pixels |
|---|---|---|---|---|---|
| a | 1.2 | 0.5 | 2.5 | 3 | 7 |
| b | 27 | 10 | 50 | 24 | 59 |
| c | 78 | 27 | 300 | 53 | 138 |

**Table B1.** The parameters of distributions: $B_{av}$—the average brightness, $B_s$—the standard deviation of $B$, $B_{max}$—the highest $B$, $S_m$—the average wavelength, $\Lambda_{max}$—the longest wavelength.

The obtained distributions are in good agreement with the photos a–c of the laser spots. All the parameters in **Table B1** are growing from *"a"* to *"c"*. Especially, five groups related to the spot *"c"* confirm the existence of very long irregularities and, eventually, indicate a surface fracture.

## Author details

Vladimir S. Voitsenya[1*], Alexandra F. Bardamid[2], Martin Balden[3], Flaviu Gostin[4], Sergey V. Khovrich[1], Vladimir G. Konovalov[1], Konstantin V. Kovtun[1], Petro M. Lytvyn[5], Sergey V. Ketov[6], Dmitri V. Luzguine-Luzgin[6], Sergei I. Solodovchenko[1], Anatoly N. Shapoval[1], Anatoly F. Shtan'[1], Vladislav N. Bondarenko[1], Ivan V. Ruzhkov[1], Ol'ga O. Skoryk[1] and Andrei A. Vasil'ev[1]

*Address all correspondence to: voitseny@ipp.kharkov.ua

1 National Science Center "Kharkov Institute of Physics and Technology", Kharkov, Ukraine

2 Taras Shevchenko National University of Kyiv, Kyiv, Ukraine

3 Max-Planck-Institut für Plasmaphysik, Garching, Germany

4 Leibniz-Institute for Solid State and Materials Research IFW Dresden, Dresden, Germany

5 Institute of Semiconductor Physics of NASU, Kyiv, Ukraine

6 WPI Advanced Institute for Materials Research, Tohoku University, Sendai, Japan

## References

[1] Donn´e AJH, Costley AE, Barnsley R, Bindslev H, Boivin R, Conway G, Fisher R., Giannella R, Hartfuss H, von Hellermann MG, Hodgson E, Ingesson LC, Itami K, Johnson D, Kawano Y, Kondoh T, Krasilnikov A, Kusama Y, Litnovsky A, Lotte P, Nielsen P, Nishitani T, Orsitto F, Peterson BJ, Razdobarin G, Sanchez J, Sasao M, Sugie T, Vayakis G, Voitsenya V, Vukolov K, Walker C, Young K, and the ITPA Topical Group on Diagnostics. Mint: Chapter 7: Diagnostics. Nucl. Fusion. 2007;47:337–384.

[2] Behrisch R, Federichi G, Kukushkin A, Reiter D. Mint: J. Nucl. Mater . 2003;388;313–316.

[3] Perez-Bergquist AG, Bei H, Zhang Y, Zinkle SJ. Mint: Fusion Reactor Materials Program, June 30, 2013;54 :154–161. DOE/ER-0313/54.

[4] Perez-Bergquist AG, Bei H, Brechtl J, Zinkle SJ. Mint: ORNL Fusion Mater. FY. 2014 ; 9–11. ORNL/TM-2014/447.

[5] Voitsenya VS, Konovalov VG, Shtan' AF, Solodovchenko SI, Becker MF, Bardamid AF, Yakimov KI, Gritsyna VT, Orlinskij DV. Mint: Rev. Sci. Instr. 1999;70:790–793.

[6] Brindley GW, Brown G, editors. Crystal Structures of Clay Minerals and their X-ray Identification. Mineralogical Society, 41 Queen's Gate, London: SW7 5HR; 1980. 495 p.

[7] Palik ED, editor. Handbook of Optical Constants of Solids. Academic Press, San Diego; 1985. 804 p.

[8] Tolansky S. High Resolution Spectroscopy (in Russian). Moscow, IL; 1955 . 380 p.

[9] Bardamid AF, Belyaeva AI, Bondarenko VN, Galuza AA, Kolesnyk OG, Konovalov VG, Naidenkova DI, Ryzhkov IV, Shapoval AN, Skinner CH, Shtan AF, Solodovchenko SI, Voitsenya VS, Yakimov KI. Mint: Phys. Scr. 2006;73:1–5.

[10] Voitsenya VS, Bakai AS, Bardamid AF, Konovalov VG, Kovtun KV, Naidenkova DI, Ryzhkov IV, Shtan' AF, Solodovchenko SI, Trembach OV, Vasil'ev AA. Mint: J. Plasma Fusion Res. SERIES. 2009;8:1379–1384.

[11] Yamamura Y, Tawara H. Mint: Atomic Data Nucl. Data Tables. 1996;62:149–253.

[12] Wanderka N, Wei Q, Sieber I, Czubayko U, Macht MP. Mint: Mater. J. Metast. Nanocryst. Mater. 1999;2-4:369–374, and references there.

[13] Bardamid A, Bryk V, Konovalov V, Orlinskij DV, Shtan' A, Shapoval A, Solodovchenko S, Voitsenya V, Yakimov K, Zakharenko N. Mint: Vacuum. 2000;58:10–15.

[14] Orlinski D, Voitsenya V, Vukolov K. Mint: Plasma Device Operations, 2007;15:33–75.

[15] Golovanivsky KS, Dugar-Jhabon VD, Schepilov VD, Safonov SA. Mint: Sov. J. Plasma Phys. 1981;7:324–333.

[16] Verbeek DH, Poschenrieder W, Carlson A, Fu J-K, McCormick K, Tsois N, Soldner FX, and the ASDEX Team. Mint: Plasma Phys. Control. Fusion. 1990;32:651–658.

[17] Miura FY and the JFT-2M team. Mint: Nucl. Fusion. 1997;37:175–188.

[18] Bardamid AF, Voitsenya VS, Davis JW, Konovalov VG, Kovtun KV, Ryzhkov IV, Shtan' AF, Solodovchenko SI, Trembach OV, Vasil'ev AA, Breuer U, Litnovsky A. Mint: J. Alloys & Compounds. 2012;514:189–194.

[19] Suh D, Asoka-Kumar P. Mint: Acta Materialia 2002; 50:537–551.

[20] Voitsenya VS, Bardamid AF, Belyaeva AI, Bondarenko VN, Galuza AA, Konovalov VG, Ryzhkov IV, Savchenko AA, Shapoval AN, Shtan' AF, Solodovchenko SI, Yakimov KI. Mint: Plasma Devices Operations. 2009;17:144–154.

[21] Eckstein W, Garcia-Rosales C, Roth J., Ottenberger W. Technical Report IPP 9/82, Max-Planck-Institut für Plasmaphysik, Garching, Germany, 1993. 342 p.

[22] Bardamid AF, Bondarenko VN, Davis JW, Konovalov VG, Lytvyn O, Ryzhkov IV, Shapoval AN, Shtan' AF, Solodovchenko SI, Voitsenya VS. Mint: J. Nucl. Mater. 2010;405:109–117.

[23] Bardamid AF, Belyaeva AI, Davis JW, Dobrovorskaya MV, Galuza AA, Kapitonchuk LM, Konovalov VG, Ryzhkov IV, Shtan' AF, Slatin KA, Solodovchenko SI, Voitsenya VS. Mint: J. Nucl. Mater. 2009;393:473–480.

[24] Konovalov VG, Makhov MN, Shapoval AN, Ryzhkov IV, Shtan' AF, Solodovchenko SI, Voitsenya VS. Mint: Probl. Atomic Sci. Technol. Ser. Plasma Phys. 2009;15:1;13–15.

[25] Kiene M, Strunskus T, Hasse G, Faupel F. Oxide formation on the bulk metallic glass $Zr_{46.75}Ti_{8.25}Cu_{7.5}Ni_{10}Be_{27.5}$. Mater. Res. Soc. Symp. Proc. 1999;554:167–172.

[26] Bardamid AF, Voitsenya VS, Lytvyn OS, Lytvyn PM, Konovalov VG, Shapoval AN, Solodovchenko SI, Yakimov KI. Mint: J. Nucl. Mater. 2008;376:125–127.

[27] Behrisch R. (Ed.), Sputtering by Particle Bombardment II, Springer-Verlag, Berlin–Heidelberg–New York–Tokyo, 1983 (Chapter 7, p. 360 in the Russian version, published by Moscow branch of Mir,1986).

[28] Atanassova E, Lytvyn P, Dub SN, Konakova RV, Mitin VF, Spassov D. Mint: J. Phys. D: Appl. Phys. 2012;45:475304 (13 pp).

[29] Tyagi AK, Nandedkar RV, Krishan K. Mint: J. Nucl. Mater. 1983;114:181–189.

[30] Tyagi AK, Nandedkar RV, Krishan K. Mint: J. Nucl. Mater. 1983;116:29–39.

[31] Tyagi AK, Nandedkar RV. Mint: J. Nucl. Mater. 1987;148:72–75.

[32] Voitsenya VS, Balden M, Bardamid AF, Bondarenko VN, Davis JW, Konovalov VG, Ryzhkov IV, Skoryk OO, Solodovchenko SI, Zhou Z-J. Mint: Nucl. Instrum. Methods Phys. Res. 2013;B302:32–39. [http://dx.doi.org/10.1016/j.nimb.2013.03.005]

IntechOpen